Aquaculture 594 (2025) 741385

Contents lists available at ScienceDirect

Aquaculture

journal homepage: www.elsevier.com/locate/aquaculture

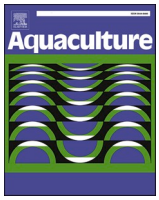

Unravelling the intricate language of fish guts: Impact of plant-based vs. plant-insect-poultry-based diets on intestinal pathways in European seabass

Ivana Bušelić [a,*], Željka Trumbić [b], Jerko Hrabar [a], Ivana Lepen-Pleić [a], Tanja Šegvić-Bubić [a], Elisavet Kaitetzidou [c], Emilio Tibaldi [d], Ivana Bočina [e], Leon Grubišić [a], Elena Sarropoulou [c]

[a] Laboratory of Aquaculture, Institute of Oceanography and Fisheries, Šetalište Ivana Meštrovića 63, 21000 Split, Croatia
[b] University Department of Marine Studies, University of Split, Ulica Ruđera Boškovića 37, 21000 Split, Croatia
[c] Institute of Marine Biology, Biotechnology and Aquaculture, Hellenic Centre for Marine Research Crete, Thalassocosmos, Gournes Pediados 2214, 71003 Heraklion, Greece
[d] Department of Agri-Food, Environmental and Animal Science, University of Udine, Via delle Scienze 206, 33100 Udine, Italy
[e] Faculty of Science, University of Split, Ulica Ruđera Boškovića 33, 21000 Split, Croatia

ARTICLE INFO

Keywords:
RNA-Seq
Intestinal metabolism
Lipid metabolism
Alternative feed
Nutrigenomic

ABSTRACT

The long-term sustainability of aquaculture depends on finding economically viable and environmentally friendly feed ingredients to reduce the use of fishmeal and fish oil. An optimal strategy for the industry is not to identify substitutes or alternatives, but to find a combination of complementary raw materials that together meet the specific nutritional requirements for a given farmed fish species. The study aimed to examine the effects of different diets on the pyloric caeca and distal intestine of subadult European seabass (*Dicentrarchus labrax*) by applying transcriptomics and transmission electron microscopy. The study examined three dietary approaches: the classic fishmeal-based diet, a plant-based diet, and a plant-insect-poultry-based diet. The distal intestine was more sensitive to dietary changes than the pyloric caeca. The differentially expressed genes in both experimental diets were mainly involved in the digestion and absorption of proteins, fats, and vitamins. The overall transcriptomic changes were greater in the plant-based group than in the plant-insect-poultry-based group and included a greater number of overrepresented metabolic and signalling pathways. In contrast to the transcriptomic results, the ultrastructural findings showed decreased inflammation and/or evidence of tissue repair in the plant-based group, particularly in the pyloric caeca. Since the nutritional quality of all fish groups in this study was previously evaluated positively, the detected transcriptome-level changes can serve as evidence supporting the efficient nutrient utilisation and adaptability in European seabass. The study provides valuable insight into the potential benefits and implications of these dietary modifications on intestinal health and pathway regulation in European seabass. This can serve as a basis for further development of sustainable European seabass aquaculture practices and optimisation of diet formulations.

1. Introduction

The long-term sustainability of aquaculture depends largely on finding economically viable and environmentally friendly feed ingredients to reduce the use of fishmeal and fish oil as the current basis of aquaculture feed (Gatlin et al., 2007; Soliman et al., 2017). An optimal strategy for the industry is not to identify substitutes or alternatives, but instead to find a combination of complementary raw materials that together meet the specific nutritional requirements for a given farmed fish species (Turchini et al., 2019). The nutritional value of farmed fish is related to their nutritional profile, i.e., their protein, fat, vitamin, and mineral content. If the diet meets the essential amino acid/protein requirements, the protein and amino acid content of fish muscle should remain conserved (Alasalvar et al., 2002; Glencross et al., 2020). This suggests potential for adjustment and flexibility in the composition of the farmed fish diet. However, differences in the amino acid profiles of fish fillets were found when plant and certain animal protein components of feed were compared with fishmeal (Kaushik et al., 2004;

Abbreviations: CF, fishmeal-based diet; CV, plant-based diet; DI, distal intestine; PC, pyloric caeca; VH10P30, a diet containing plant proteins, black soldier fly meal and poultry by-product..

* Corresponding author.
E-mail address: buselic@izor.hr (I. Bušelić).

https://doi.org/10.1016/j.aquaculture.2024.741385
Received 31 January 2024; Received in revised form 2 May 2024; Accepted 21 July 2024
Available online 25 July 2024

Rasmussen, 2001). This highlights the importance of informed decision-making processes to balance fish health, consumer satisfaction, and environmental sustainability of feed ingredients.

In contrast to proteins, the lipid content of the fillet, especially the fatty acid composition, is influenced by the diet (Stone et al., 2011). Fillet lipid content can be altered by changes in feed intake, dietary lipid content, and protein-to-lipid or protein-to-energy ratio, and it increases as fish grow (Glencross et al., 2020). However, the effects of alternative lipid sources on fillet fat content are less pronounced than on fatty acid composition. The nutritional quality of farmed fish is directly related to the content of long-chain omega-3 polyunsaturated fatty acids (n-3 LC-PUFA), such as eicosapentaenoic acid (EPA, 20:5n3) and docosahexaenoic acid (DHA, 22:6n3) (Leaver et al., 2008a). Fish is considered one of the most important sources of these fatty acids for humans (Calder, 2014), along with krill and algal oils (FAO/WHO, 2008; WHO, 2003).

To facilitate informed dietary choices, the European Food Safety Authority (EFSA) has issued typical values for fat, fatty acids, and cholesterol in some animal-derived foods. European seabass (*Dicentrarchus labrax*) falls into the lean fish category (<2 g fat/100 g fish), and the expected values of PUFAs for this fish category are: 0.07 g EPA/100 g fish, and 0.20 g DHA/100 g fish (EFSA, 2010). Unlike freshwater fish, marine fish species have limited ability to convert α-linolenic acid (ALA, 18:3n3) to EPA and DHA fatty acids (Tocher, 2003; Watanabe, 1982), and so it is a challenge for the aquaculture industry to maintain the content of EPA and DHA in farmed fish fillets. This is especially true as the proportion of alternative vegetable oil sources in fish feed formulations increases and the ratio of n-3 to n-6 fatty acids changes (Tocher, 2015). For example, linoleic acid (LA, 18:2n6), which is abundant in vegetable oils often used as substitutes for fish oil, significantly increases the LA content in fish fillets (Sprague et al., 2016), and a decreased ratio of n-3 to n-6 LC-PUFA is not considered beneficial from a human health perspective (Calder, 2014; Sprague et al., 2016).

European seabass, one of the cornerstone species of Mediterranean aquaculture, has very low fatty acid bioconversion rates, although the enzymes involved in elongation and desaturation of 18C fatty acids, namely D-5 elongase and D-6 desaturase, have been indirectly detected in this species (Mourente et al., 2005). This implies that a relatively high intake of n-3 LC-PUFA is required for farmed seabass (Turchini et al., 2009), which is the reason for the historical reliance on fishmeal and fish oil for this resource-intensive carnivorous species (FAO, 2018). Today, farmed European seabass is one of the most economically and culturally important marine fish species in the European Union, with aquaculture accounting for over 96% of total production (Vandeputte et al., 2019). Many plant-based ingredients have been investigated as partial substitutes for fishmeal and fish oil in seabass without affecting survival, growth, or gut health (Bonvini et al., 2018; Kaushik et al., 2004; Torrecillas et al., 2017), although complete replacement of fishmeal significantly reduced seabass growth and upregulated gene expression in the gut-associated immune system (Torrecillas et al., 2017). Plant proteins are often associated with lower palatability, digestibility challenges (Bonaldo et al., 2008; Tibaldi et al., 2006), a suboptimal fatty acid profile (Morris et al., 2005), and the presence of anti-nutritional factors (Abdel-Latif et al., 2022).

Aside from plant-based substitutes, other protein sources have attracted the attention of the aquaculture industry and nutritionists. Processed animal proteins, such as poultry byproducts, are palatable to farmed fish and have high-quality protein content and high mineral content (Campos et al., 2018; Galkanda-Arachchige et al., 2020). However, the availability of essential amino acids such as methionine and lysine is lower compared to fishmeal (Karapanagiotidis et al., 2019) and poultry fat is rich in n-6 fatty acids but poor in n-3 LC-PUFA (Campos et al., 2019). On the other hand, black soldier fly (*Hermetia illucens*) larvae meal has a balanced essential amino acid profile similar to that of fishmeal, with a high protein, vitamin and mineral content (Nogales-Mérida et al., 2019). The fatty acid content of insect meal depends on the composition of substrate used to grow the insects and their developmental stage (Boukid et al., 2021). Usually, insect meal contains higher levels of n-6 polyunsaturated fatty acids, but insufficient amounts of EPA and DHA (Tran et al., 2015). Most studies on European seabass have been conducted on juvenile fish using either black soldier fly larvae meal (Abdel-Latif et al., 2021; Abdel-Tawwab et al., 2020; Mastoraki et al., 2020) or pre-pupae meal (Magalhães et al., 2017; Moutinho et al., 2021; Zarantoniello et al., 2023), with successful replacement of fishmeal by 20–50% without affecting fish health, growth performance, feed conversion or digestibility. A 20% supplementation with black soldier fly pre-pupae meal did not affect fillet quality characteristics (colour and fatty acid profile) and possibly preserved fillet from lipid oxidation, either alone (Moutinho et al., 2021) or enriched with spirulina (Zarantoniello et al., 2023).

In a previous study on subadult European seabass, we applied a multidisciplinary approach to compare the effects of a vegetable protein-based diet, in which different proportions of the vegetable protein mixture were replaced with partially defatted black soldier fly pupae meal alone or in combination with poultry byproduct meal (PBM) (Lepen Pleić et al., 2022). Besides plant-based diets, a fishmeal-based diet and a fishmeal-based diet supplemented with partially defatted black soldier fly pupae meal were also assessed. For their effects on growth performance, muscle tissue composition, skin coloration, gut morpho-physiology, digestive enzyme activities, gut microbiota, and feed cost relative to growth. That study reported that the plant-based diet combined with black soldier fly and poultry-by-product derived proteins (VH10P30 diet) outperformed both fishmeal-based (CF) and plant-based (CV) diets in terms of growth and feeding efficiency of subadult European seabass with a higher final body weight, daily gain, and specific growth rate, while the feed conversion ratio was significantly lower. In addition, the observed changes in intestinal histomorphology caused by the CV diet were less pronounced with the addition of black soldier fly pupae and poultry by-product meal in the VH10P30 diet (Lepen Pleić et al., 2022).

To build the basis for an in-depth, knowledge-based understanding of the observed effects, the aim of the present study was to explore the effects of these diets at the cellular level by providing transcriptomic nutrigenomic profiling of the intestine of subadult European seabass and the ultrastructure of the studied intestinal parts using transmission electron microscopy (TEM).

2. Material and methods

2.1. Experimental design and feed formulation

The feeding trial was conducted with subadult European seabass brought from a local farm to the Laboratory of Aquaculture facilities at the Institute of Oceanography and Fisheries in Split, Croatia. Experimental procedures involving animals in this study were conducted in accordance with the Laboratory Animal Management Principles of Croatia. All experimental protocols were approved by the Ethics Committee of the Institute of Oceanography and Fisheries (No. 134/2/2018). A detailed description of the experimental setup is available in (Lepen Pleić et al., 2022). Briefly, during the two-week acclimation period in an open-flow system with adjacent coastal water supply, fish were fed a commercial diet (OptibassL-2, Skretting, Spain; 48.5% protein, 16% lipids, 3.7% fibre, 6.4% ash, expressed in as-fed basis). After weighing and measuring, 550 fish were randomly distributed among 10 tanks each with a capacity of 2600 l and containing 55 animals. There were two randomly assigned tanks for each feeding treatment, and the initial mean body weight (± SD) of 149 ± 21 g was not significantly different between tanks ($F = 0.71$, $df = 9$, $p = 0.7$). Two of these feeding treatments were not explored here.

In the present study, three isoproteic (45%), isolipidic (20%) and grossly isoenergetic (20.3 MJ kg^{-1}) formulations were selected for a comprehensive exploration of the European seabass intestine using transcriptomics and TEM. The ingredient and nutrient composition of

the test diets used in this study are given is Tables 1 and 2. Briefly, a positive control diet rich in fish meal and fish oil (CF) was formulated to obtain a 15:85 weight ratio between vegetable and marine proteins and 67:33 weight ratio between fish and non-fish lipids. A plant protein-rich diet (CV) was designed to obtain opposite ratios between protein and lipid sources (e.g., 85:15 weight ratio between vegetable and marine proteins and a 33:67 weight ratio between fish and non-fish lipids), as calculated from the crude protein and lipid contribution to the whole diet of all marine and non-marine dietary ingredients. In the VH10P30 diet, 10 and 30% of crude protein from the mixture of purified vegetable protein sources of the CV preparation (including wheat gluten, corn gluten and soy protein concentrate) were replaced by crude protein from *Hermetia illucens* meal and poultry by-product meal (PBM) respectively, while maintaining the same levels of less purified plant protein sources, such as soybean and rapeseed meals, as well as a 33:67 fish to non-fish lipid ratio as in the CV diet. All feeds were commercially produced by SPAROS Lda in Portugal and were formulated to meet all known nutritional requirements of subadult European seabass (Kaushik, 2002).

Table 1
Ingredient composition (g 100 g^{-1}) and proximate (% as fed) of the test diets used for subadult European seabass.

Ingredient composition	CV	VH10P30	CF
Fish meal[1]	–	–	16
Fish meal[2]	4	4	45
Vegetable-protein mix 1[3]	41	13.1	6
Vegetable-protein mix 2[4]	20	20	
Hermentia illucens meal[5]	–	8	–
PBM[6]	–	20.2	–
Feeding stimulants[7]	5.5	5.5	–
Wheat meal*	1	6.7	5.7
Whole peas*	6.7	5	11
Fish oil[8]	6	6	8
Vegetable oil mix[9]	11.5	7.7	6.4
Vitamin & Mineral Premix[10]	0.3	0.3	0.3
Choline HCL	0.1	0.1	0.1
Sodium phosphate (NaH2PO4)	1.6	1.6	–
L –Lysine[11]	0.4	–	–
DL-Methionine[12]	0.4	0.3	–
Celite	1.5	1.5	1.5
Proximate composition			
Crude protein (N x 6.25)	45.2	45.1	45.4
Crude lipid	20.1	20.2	20.2
Starch[13]	6.2	7.6	8.6
Carbohydrate[14]	23.2	19.5	17.8
Moisture	4.4	5.7	4.7
Ash	7.1	9.5	11.9
Gross energy, MJ/kg DM	23.0	22.9	22.8

Part of this table was published in (Lepen Pleić et al., 2022).

[1] Fishmeal Super Prime, Pesquera Diamante Peru (66.3% crude protein (CP), 11.5% crude fat (FC)).

[2] Fishmeal by-product Conresa 60, Conserveros Reunidos S.A. Spain (61.2% CP, 8.4% FC).

[3] Vegetable-protein source mixture 1: soy protein concentrate-Soycomil, 49%; wheat gluten, 29%; corn gluten%, 22.

[4] Vegetable-protein source mixture 2: dehulled solvent extracted soybean meal, 65%; defatted rapeseed meal, 35%.

[5] ProteinX™, Protix, Dongen, The Netherlands (CP, 55.4%; FC, 20.8% as fed).

[6] Poultry by-product meal from Azienda Agricola Tre Valli; Verona, Italy (CP, 65.6%; FC, 14.8% as fed).

[7] Feeding stimulants: fish protein concentrate CPSP90- Sopropeche, France (82.6% CP), 64; Squid meal (80.3% CP), 36.

[8] Fish oil: from pelagic forage fish, Sopropêche, France.

[9] Vegetable oil mix: rapeseed oil, 56%; linseed oil, 26%; palm oil, 18%.

[10] Vitamin and mineral supplement (per kg of premix): Vit. A, 2,000,000 IU; Vit D3, 200,000 IU; Vit. E 30,000 mg; Vit. K3, 2500 mg; Vit.B1, 3000 mg; Vit. B2, 3000 mg: Vit B3, 20,000 mg; Vit. B5, 10,000 mg; Vit B6, 2000 mg, Vit. B9, 1500 mg; Vit. B12, 10 mg, Biotin, 300 mg; Stay C®, 90,000 mg; Inositol, 200,000 mg; Cu, 900 mg; Fe, 6000 mg; I, 400 mg; Se, 40 mg; Zn, 7500 mg.

[11] L—lysine, 99%; Ajinomoto EUROLYSINE S.A.S; France.

[12] DL—Methionine: 99%; EVONIK Nutrition & Care GmbH; Germany.

[13] Calculated from the starch content of single ingredients.

[14] Calculated by difference.

* The ingredients were obtained from local providers by Sparos Lda.

Table 2
Protein and lipid content (% as fed), essential amino acid composition (g/kg as fed) of ingredients used to formulate the test diets for subadult European seabass.

Protein origin (%)	CV	VH10P30	CF
Fish	15	15	85
PBM	–	30	–
Hermentia illucens	–	10	10
Protein from veg mix + AA	85	45	5
Amino acid (AA) composition (g/kg)			
Essential AA composition			
Arginine	27.4	29.4	24.7
Histidine	10.7	10.1	11.2
Isoleucine	18.5	15.5	16.7
Leucine	38.0	31.8	29.2
Lysine	25.2	23.3	29.4
Methionine + cysteine	18.1	16.8	13.0
Phenylalanine + tyrosine	35.7	31.4	34.8
Threonine	16.2	17.1	16.4
Tryptophan	4.4	4.5	4.7
Valine	20.4	20.8	19.6
Non-essential AA composition			
Aspartic acid	34.5	39.4	34.0
Glutamic acid	91.3	75.5	53.5
Alanine	20.8	25.6	24.3
Glycine	20.0	28.8	27.8
Proline	31.7	29.6	20.1
Serine	21.1	19.8	16.4
Lipid origin (%)			
Fish	34	34	66
Lipid from alternate ingredients	66	66	34

Part of this table was also published as Supplementary Material in (Lepen Pleić et al., 2022).

The experiment lasted 22 weeks, and feed rations were adjusted after monthly weighing and measuring. Fish were hand-fed twice daily (8:00 a.m. and 4:00 p.m.) to apparent satiation, and feed intake and water parameters were measured daily. Adjacent coastal waters were supplied continuously at a flow rate of 15 l min^{-1} and further aerated with air pumps after passing through the mechanical filtration system. Since the experiment lasted from July to December 2019, the natural photoperiod ranged from 14.42 to 9.12 h of daylight. Water temperature ranged from 24.5 ± 0.9 °C during July–August to 17.2 ± 1.4 °C during November–December, dissolved oxygen content ranged from 6.0 to 7.5 mg l^{-1}, and salinity ranged from 37.2 to 38‰. Complete daily measurements of water temperature and dissolved oxygen content are presented in Fig. S1.

2.2. Sample collection, RNA extraction, and Illumina next-generation sequencing

The fish were not fed on the morning of the final sampling day. The fish were administered an overdose of the anaesthetic MS-222 (100 mg ml^{-1}, Sigma Aldrich, Saint-Louis, MO, USA) and samples were collected from the gastrointestinal tract of five fish per tank. The gastrointestinal tract samples were carefully rinsed with autoclaved seawater to remove residual faeces and pyloric caeca (PC) and distal intestine (DI) subsamples taken from the same fish, and stored in RNAlater (Qiagen, Hilden, Germany) at −20 °C until RNA extraction. The area after the ileo-rectal valve was considered distal intestine and we always sampled the middle part after the ileo-rectal valve. The correct sampling of the DI was supported by the appearance of short, simple (or fused) villi with a high number of goblet cells in histological slides. Total RNA was

extracted using Tri Reagent (Ambion Inc., Invitrogen, Carlsbad, CA, USA) according to the manufacturer's protocol and dissolved in 20 μl of RNase/DNase-free water (Merck Millipore, Billerica, MA, USA). Integrity was assessed for all isolated RNA samples by agarose (1%) gel electrophoresis, before being sent on dry ice to the Institute of Marine Biology, Biotechnology and Aquaculture (IMBBC) of the Hellenic Centre for Marine Research (HCMR), Greece, in September 2020. RNA concentration, purity, and integrity were determined by ND-1000 Nanodrop spectrophotometer measurements (Thermo Fisher Scientific, Waltham, MA, USA) as well as by RNA 6000 Pico Kit electrophoresis (2100 Bioanalyzer, Agilent Technologies, Santa Clara, CA, USA). Based on the quality, 24 samples of total RNA were selected for cDNA library preparation, which included four biological replicates (two from each tank) per feeding treatment from two selected tissues (PC and DI). In this study, one biological replicate corresponded to the same fish specimen, i.e., PC and DI were paired as subsamples. The cDNA library was prepared according to the manufacturer's protocol, using the QuantSeq 3' mRNA-Seq Library Prep Kit REV for Illumina (Moll et al., 2014). QuantSeq is a robust and simple mRNA sequencing method. It increases the precision of gene expression measurements by generating only one fragment per transcript. At lower read depths, such focus on the 3′ end leads to higher stability of differential gene expression measurements (Corley et al., 2019). Single-end 1 × 75 3'UTR sequencing was performed by applying the Illumina HiSeq 2000 platform (Illumina, San Diego, CA, USA).

2.3. Pre-processing of raw RNA-Seq data, mapping, and differential expression analyses

Raw data were submitted to the NCBI Sequence Read Archive (SRA) under BioProject accession number PRJNA956721. In total, 24 samples of European seabass intestine (DI) comprised an average of 7.1 million reads per library (Table 3). Detailed information on raw reads obtained per sample, and the number of reads after filtering and mapping are given in Table S1. The quality of the data throughout processing was assessed using FastQC v0.11.8 (Babraham Bioinformatics, Babraham Institute, Cambridge, UK). Residual ribosomal RNA (rRNA) contamination was assessed and filtered out using rRNA sequences provided by SortMeRNA v4.3.6 (Kopylova et al., 2012). Trimmomatic v 0.39 (Bolger et al., 2014) was used for Illumina adapter and low quality reads trimming. Sliding window clipping of reads was set to scan the read with a 4-base wide sliding window, cutting when the average quality per base dropped below 20. All reads were trimmed at base 74 and reads shorter than 40 bases were removed. On average, 90.4% of reads were retained after trimming. STAR v2.7.10b (Dobin et al., 2013) was used to align reads within RSEM v 1.3.3 (Li and Dewey, 2011) to European seabass transcriptome available from Ensembl release 109 (Howe et al., 2021). On average, 88.1% of reads were uniquely mapped (Table 1 and Table S1). Gene level count data from RSEM v 1.3.3 (Li and Dewey, 2011) were imported into R v4.2.2 (R Core Team, 2021) using the tximport package (Soneson et al., 2016). Differential analysis of gene expression was performed using the DESeq2 package (Love et al., 2014) of the Bioconductor v3.17 (Gentleman et al., 2004). Features with low expression (with less than one read per sample, summed to at least three reads across three samples) were filtered out before analysis. After an initial exploratory analysis of the data using principal component analysis (PCA) (Fig. 1), we performed two separate analyses for PC and DI and to remove one outlier sample for each tissue. Differentially expressed genes (DEGs) were identified at Benjamini-Hochberg false discovery rate (FDR) < 0.05. For each gene, a generalised linear model was fitted with a design that included experimental feed as a factor. Two of the three generated contrasts using the Wald test were further explored in the enrichment analysis: VH10P30 vs. CF and CV vs. CF, i.e., the CF group was the control feed in both the PC and DI analyses. We performed an additional analysis comparing VH10P30 vs. CV group as a negative control for both PC and DI, but the enrichment analysis did not yield any significant results.

Table 3
Statistics about data pre-processing, read mapping and annotation summary.

Pre-processing and mapping information	
Average reads per sample	7,142,234
Trimmed reads	6,458,282
Uniquely mapped reads	5,688,714
Total genes	24,030
Annotation report	
UniProtKB/Swiss-Prot	21,270
KEGG (KO)	15,304
GO (EggNOG)	12,973
Unique UniProt symbols in GAGE analysis for PC (out of 16,136 genes)	11,754
Unique KEGG (KO) identifiers in GAGE analysis for PC	7306
Unique UniProt symbols in in GAGE analysis for DI (out of 17,304 genes)	12,279
Unique KEGG (KO) identifiers in GAGE analysis for DI	7525

2.4. Functional annotation and enrichment analysis

Coding sequences were annotated using the blastp algorithm (e-value cut-off of 10^{-5}) implemented in BLAST+ v2.9.0 (Camacho et al., 2009) against the UniProtKB/Swiss-Prot database (UniProt Consortium, 2015). The web version of eggNOG (evolutionary genealogy of genes: Non-supervised Orthologous Groups) (Cantalapiedra et al., 2021) was used to retrieve annotations, including GO (Gene Ontology) and KEGG (Kyoto Encyclopedia of Genes and Genomes) ortholog identifiers (KO). Functional analysis of KEGG signalling and metabolic pathways was performed using GAGE (Generally Applicable Gene set Enrichment) as implemented in the gage package (Luo et al., 2009) for R v4.2.2 (R Core Team, 2021). Log (base 2)-fold changes were extracted from the results generated by DESeq2 (Love et al., 2014), and the sets of DEGs were tested against all expressed genes (after removing low-count features) as the background (Table 1). Testing was performed for bidirectionally perturbed pathways using the q-value cut-off of 0.05. Following the GAGE analyses, the Pathview package (Luo and Brouwer, 2013) was used to visualise DEGs (Benjamini-Hochberg false discovery rate (FDR) < 0.05) on their respective KEGG maps. Because the native output of KEGG maps in the Pathview package (Luo and Brouwer, 2013) is a low-resolution png image, selected metabolic KEGG maps were redrawn in Adobe InDesign (Adobe Systems, San Jose, CA, USA).

2.5. Transmission electron microscopy (TEM)

Small pieces of tissue from PC and DI were dissected and fixed in 2.5% glutaraldehyde/2% paraformaldehyde in 0.1 M phosphate buffer (PB) at 4 °C overnight. Samples were then washed in 0.1 M PB with 4% glucose (3 × 15 minutes) and post-fixed in 1% aqueous osmium tetroxide for 2 h at room temperature. After washing in deionised water (3 × 15 min), samples were dehydrated in ascending acetone series (30—100%, 15 min each) and infiltrated for 1 h with 25, 50 and 75% mixtures of anhydrous acetone and low viscosity Spurr resin (SPI Chem, West Chester, PA, USA). Finally, the samples were left in pure resin in the desiccator overnight, transferred to embedding moulds, and polymerised for 48 h at 60 °C. Semithin sections (500 nm) were stained with 1% toluidine blue and examined for orientation under the light microscope. Ultrathin sections (60–70 nm) were placed on Formvar-coated 100-mesh copper grids, stained with uranyl acetate and lead citrate (Reynolds, 1963), and observed in a Jeol JEM-1400Flash microscope at an accelerating voltage of 100 kV. Images were taken with a Matataki Flash sCMOS camera and assembled and annotated in Adobe PhotoShop CS5 (Adobe Systems, San Jose, CA, USA). As the best quality images were selected, fish samples chosen as treatment representatives are not necessarily the same as those selected for transcriptome sequencing.

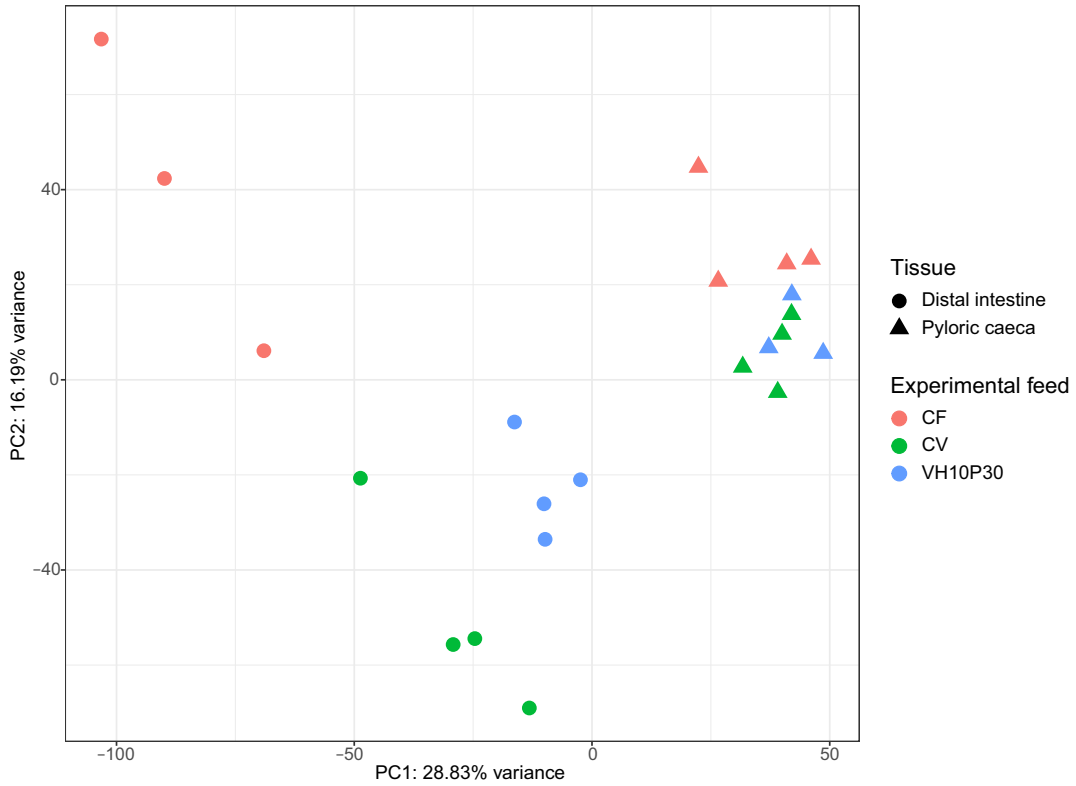

Fig. 1. PCA plot. Grouping of samples by gene expression variation in the pyloric caeca and distal intestine of subadult European seabass after feeding trial (groups VH10P30, CV and CF). Raw counts were log normalised by variance stabilising transformation, and profiles were plotted using principal component analysis (PCA).

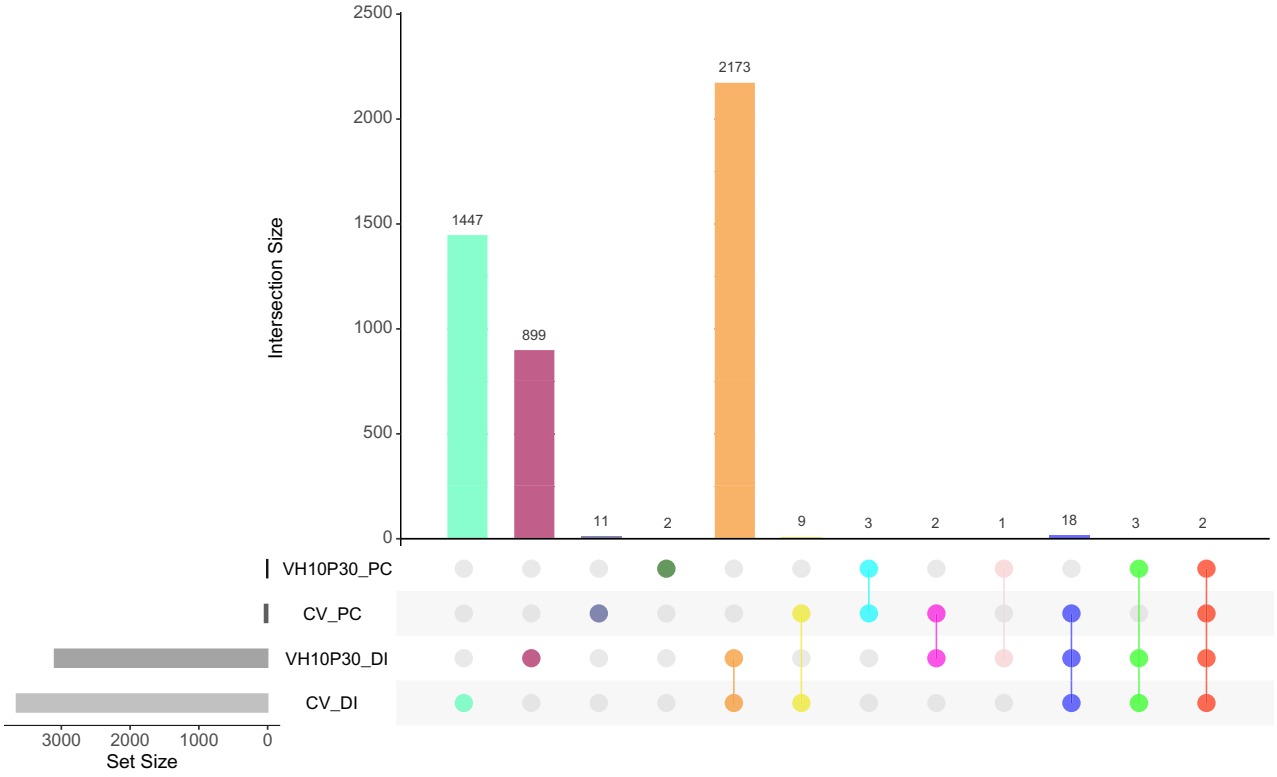

Fig. 2. UpSet plot. The total number of differentially expressed genes (DEGs) for each comparison is shown on the left in a horizontal grayscale bar plot: CV vs. CF for pyloric caeca (PC) and distal intestine (DI) and VH10P30 vs. CF for PC and DI of subadult European seabass. Vertical bar plot shows the number of unique DEGs for each dataset and the number of shared DEGs for each combination in colour.

3. Results

3.1. Interpretation of PC and DI transcriptomes

Pyloric caeca (PC) and distal intestine (DI) of the subadult European seabass responded differently to the experimental treatments (Fig. 1). In both VH10P30 vs. CF and CV vs. CF comparisons, PC showed low numbers of differentially expressed genes (DEGs), in contrast to DI. This suggests a lack of systematic evidence of dietary influence on PC transcriptomes (Fig. 2).

Of the 11 DEGs in PC in the VH10P30 group, 4 were upregulated and 7 downregulated. Among them, two genes—*inactive all-trans-retinol 13,14-reductase* (*rtstl*) and *methylsterol monooxygenase 1* (*msmo1*)—were also upregulated in PC of the CV group and in DI in both experimental treatments (VH10P30 and CV), depicted in light red in Fig. 2 and detailed in Table S2 and Table S3. *Pro-interleukin-16* (*il16*) was upregulated in the VH10P30 (Table S2) and CV groups for PC (Table S3) but not DI.

A total of 45 (29 upregulated and 16 downregulated) DEGs were found in the PC of the CV vs. CF comparison (Table S3). Some upregulated DEGs associated with digestion included *carbonic anhydrase 1* (*cah1*), *pepsin A* (*pepa*) and *squalene monooxygenase* (*erg1*). Several other upregulated DEGs were linked to immune response, such as *il16, mamu class II histocompatibility antigen, DR alpha chain* (*dra*), *major histocompatibility complex class I-related gene protein* (*hmr1*), and *putative interleukin-17 receptor E-like* (*il17el*) (Table S3). Certain DEGs related to immunity were downregulated, such as *C-type lectin domain family 4 member E* (*clc4e*). Functional enrichment analysis identified only one bidirectionally perturbed KEGG signalling pathway in this group, neuroactive ligand-receptor interaction.

In contrast, in DI, 3098 (1541 upregulated and 1557 downregulated) DEGs were identified in the VH10P30 vs. CF group (Table S4) and 3652 (1683 upregulated and 1969 downregulated) in the CV vs. CF group (Table S5). Of those, 2173 DEGs were common to both the VH10P30 and CV groups in DI, indicating substantial overlap between these transcriptomes (Fig. 2). This observation is further supported by the overlap of overrepresented KEGG metabolic and signalling pathways shown in Fig. 3, especially bidirectionally perturbed pathways directly related to digestion (protein, fat, and vitamin digestion and absorption) and the endocrine system (e.g., the PPAR signalling pathway). Accordingly, interpretation of the results of DI was particularly focused on the shared DEGs.

All of the KEGG pathways overrepresented in the VH10P30, with the exception of the pancreatic secretion pathway, were also overrepresented in the CV group, with the addition of several pathways belonging to the signalling molecules and interaction category (ECM-receptor interaction and cell adhesion molecules), lipid metabolism (steroid biosynthesis), development and regeneration (axon guidance), endocrine system (insulin secretion), and signal transduction (calcium signalling pathway). The similarities also extended to pathways not present in both groups. For example, although the pancreatic secretion pathway was significantly bidirectionally regulated only in the VH10P30 group (Table 4, Fig. S2), insulin secretion was bidirectionally perturbed in the CV group (Table 5, Fig. S3), with many DEGs shared between these pathways. Notably, genes like *cholecystokinin receptor* (*cckar*, downregulated in both pathways) and *sodium/potassium-transporting ATPase subunit alpha-1* (*at1a1*, downregulated in both pathways), and *beta-233* (*at233*, upregulated in pancreatic secretion and downregulated in insulin secretion) were shared. Even *glucagon-1* (*gluc1*), which was at the top of the list of DEGs in the CV group for insulin secretion (Table 5), was also upregulated in the VH10P30 group (Table S4).

The similarities between the two treatments (VH10P30 vs. CF and CV vs. CF) were even more pronounced in lipid metabolism, given that the vast majority of genes involved in the pathway of fat digestion and absorption were common and regulated in the same direction (Fig. 4 and

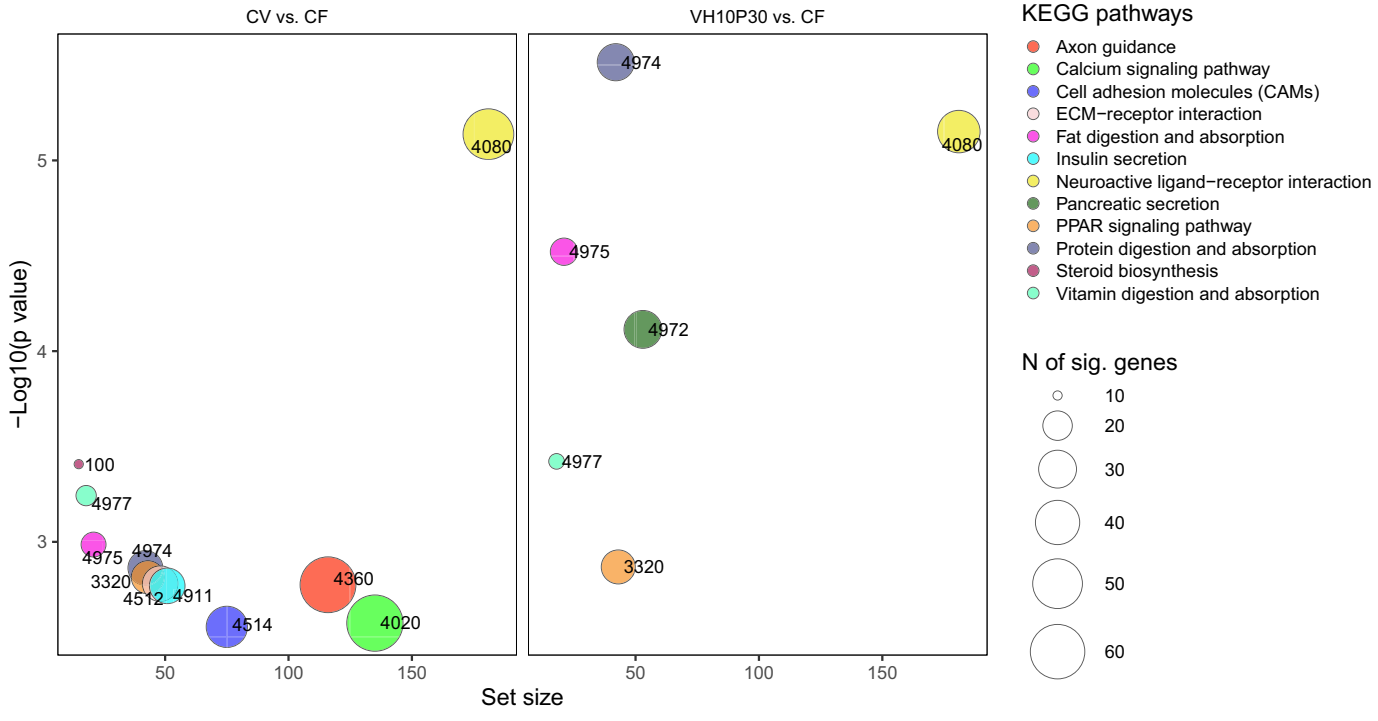

Fig. 3. Overrepresented KEGG metabolic and signalling pathways. Differentially perturbed KEGG pathways in the distal intestine of subadult European seabass after feeding trial: CV vs. CF group (left) and VH10P30 vs. CF group (right). Set size is plotted against $\log_{10}$ p-value and circle size depicts the number of differentially expressed genes (DEGs) for each pathway. Pathway IDs are shown in abbreviated form, and the full IDs are as follows: ko04360 Axon guidance, ko04020 Calcium signalling pathway, ko04514 Cell adhesion molecules (CAMs), ko04512 ECM-receptor interaction, ko04975 Fat digestion and absorption, ko04911 Insulin secretion, ko04080 Neuroactive ligand-receptor interaction, ko04972 Pancreatic secretion, ko03320 PPAR signalling pathway, ko04974 Protein digestion and absorption, ko00100 Steroid biosynthesis, ko04977 Vitamin digestion and absorption.

Table 4
DEGs in the distal intestine identified in the KEGG pancreatic digestion pathway.

Gene symbol	VH10P30 vs. CF logFC	padj	UNIPROT/SWISSPROT description
cbpa2	5.12	0.0003	*Carboxypeptidase A2*
amy	4.91	0.0000	*Alpha-amylase*
cel2a	4.84	0.0000	*Chymotrypsin-like elastase family member 2 A*
cel3b	4.61	0.0000	*Chymotrypsin-like elastase family member 3B*
ctrb	4.59	0.0000	*Chymotrypsin B*
s26a3	4.58	0.0001	*Chloride anion exchanger*
cbpb1	4.57	0.0001	*Carboxypeptidase B*
cel	4.11	0.0001	*Bile salt-activated lipase (Fragment)*
try2	4.00	0.0000	*Trypsin-2 (Fragment)*
cbpa1	3.93	0.0013	*Carboxypeptidase A1*
pg12b	3.76	0.0040	*Group XIIB secretory phospholipase A2-like protein*
s4a4	3.22	0.0000	*Electrogenic sodium bicarbonate cotransporter 1*
gna14	2.23	0.0021	*Guanine nucleotide-binding protein subunit alpha-14*
itpr3	1.98	0.0000	*Inositol 1,4,5-trisphosphate receptor type 3*
at233	1.93	0.0001	*Sodium/potassium-transporting ATPase subunit beta-233*
cd38	1.77	0.0016	*ADP-ribosyl cyclase/cyclic ADP-ribose hydrolase 1*
kpca	1.63	0.0000	*Protein kinase C alpha type*
rab25	1.46	0.0014	*Ras-related protein Rab-25*
plcb3	1.46	0.0001	*1-phosphatidylinositol 4,5-bisphosphate phosphodiesterase beta-3*
adcy3	1.20	0.0209	*Adenylate cyclase type 3*
rac1	1.01	0.0012	*Ras-related C3 botulinum toxin substrate 1*
at2a2	−0.84	0.0078	*Sarcoplasmic/endoplasmic reticulum calcium ATPase 2*
gnas	−0.97	0.0048	*Guanine nucleotide-binding protein G(s) subunit alpha*
nheb	−1.21	0.0046	*Na(+)/H(+) exchanger beta*
kpcb	−1.50	0.0049	*Protein kinase C beta type*
ryr2	−1.89	0.0022	*Ryanodine receptor 2*
b3a2	−1.98	0.0013	*Anion exchange protein 2*
at1a1	−2.02	0.0000	*Sodium/potassium-transporting ATPase subunit alpha-1*
trpc1	−2.45	0.0025	*Short transient receptor potential channel 1*
cckar	−5.51	0.0007	*Cholecystokinin receptor*

DEGs are ordered by log2-fold change (logFC) value (from largest to smallest) comparing VH10P30 vs. CF, along with the associated p-adjusted value (padj). DEGs were identified at a Benjamini-Hochberg false discovery rate (FDR) < 0.05.

Table 5
DEGs identified in the distal intestine in the KEGG insulin secretion pathway.

Gene symbol	CV vs. CF logFC	padj	UNIPROT/SWISSPROT description
gluc1	2.79	0.0000	*Glucagon-1*
gna14	2.43	0.0005	*Guanine nucleotide-binding protein subunit alpha-14*
gtr2	1.44	0.0466	*Solute carrier family 2, facilitated glucose transporter member 2*
trpm5	1.32	0.0283	*Transient receptor potential cation channel subfamily M member 5*
adcy3	1.27	0.0115	*Adenylate cyclase type 3*
itpr3	1.26	0.0025	*Inositol 1,4,5-trisphosphate receptor type 3*
kcc2d	1.17	0.0000	*Calcium/calmodulin-dependent protein kinase type II subunit delta*
kpca	0.73	0.0381	*Protein kinase C alpha type*
kapcb	−0.89	0.0001	*cAMP-dependent protein kinase catalytic subunit beta*
kpcb	−1.17	0.0297	*Protein kinase C beta type*
gnas	−1.32	0.0001	*Guanine nucleotide-binding protein G(s) subunit alpha*
vamp2	−1.49	0.0312	*Vesicle-associated membrane protein 2*
stx1b	−1.58	0.0350	*Syntaxin-1B*
at1a1	−1.78	0.0001	*Sodium/potassium-transporting ATPase subunit alpha-1*
at233	−1.80	0.0017	*Sodium/potassium-transporting ATPase subunit beta-233*
plcb1	−2.01	0.0010	*1-phosphatidylinositol 4,5-bisphosphate phosphodiesterase beta-1*
pclo	−2.06	0.0328	*Protein piccolo*
rims2	−2.24	0.0070	*Regulating synaptic membrane exocytosis protein 2*
cac1f	−2.37	0.0296	*Voltage-dependent L-type calcium channel subunit alpha-1F*
paca	−2.38	0.0160	*Glucagon family neuropeptides*
ryr2	−2.43	0.0001	*Ryanodine receptor 2*
cr3l2	−2.97	0.0020	*Cyclic AMP-responsive element-binding protein 3-like protein 2*
cckar	−3.57	0.0068	*Cholecystokinin receptor*
pacr	−3.98	0.0311	*Pituitary adenylate cyclase-activating polypeptide type I receptor*
cac1c	−3.99	0.0001	*Voltage-dependent L-type calcium channel subunit alpha-1C*
rab3a	−4.57	0.0151	*Ras-related protein Rab-3 A*

DEGs are ordered by log2-fold change (logFC) value (from largest to smallest) comparing CV vs. CF, along with the associated p-adjusted value (padj). DEGs were identified at a Benjamini-Hochberg false discovery rate (FDR) < 0.05.

Table 6). Only one gene was downregulated in both comparisons, *phospholipid phosphatase 2* (*plpp2*). In VH10P30, *apolipoprotein A-I* (*apoa1*) was upregulated in fat digestion and absorption (Fig. 4A and Table 6), PPAR signalling pathway (Fig. 5A and Table 7), and vitamin digestion and absorption (Table 8 and Fig. S4). In addition to *apoa1*, *intestinal-* and *liver-type fatty acid-binding proteins* (*fabpi* and *fabpl*) were also upregulated in fat digestion and absorption (Fig. 4A and Table 6) and PPAR signalling pathway (Fig. 5A and Table 7). Other upregulated apolipoproteins, *apolipoprotein B-100* (*apob*) and *apolipoprotein A-IV* (*apoa4*), were listed in the fat digestion and absorption (Fig. 4A and Table 6) and vitamin digestion and absorption pathways (Table 8 and Fig. S4). These apolipoproteins were also detected in the CV group, as were *fabpi* and *fabpl* which had a greater logFC/smaller p-adjusted value in the CV treatment. Other types of fatty acid-binding proteins were also activated in this test group: *fabp7* was upregulated and *fabp4* was downregulated for the PPAR signalling pathway (Table 7). The difference between the VH10P30 vs. CF and CV vs. CF groups concerning the PPAR signalling pathway is more evident in Fig. 5A and B, showing that target genes leading to gluconeogenesis and cholesterol metabolism were more affected in the VH10P30 diet. Furthermore, it is evident from the KEGG map of vitamin digestion and absorption that B12 metabolism seemed to be downregulated for both comparisons, directly related to downregulation of *cubilin* (*cubn*), and upregulation of all other vitamins (Fig. S4). *Cubn* was the only downregulated gene for vitamin digestion and absorption (logFC of −8 for VH10P30, −5.5 for CV) (Table 8).

In contrast, some DEGs were present in only the VH10P30 vs. CF analysis for DI, such as the *carboxypeptidases* (*cbpa1*, *cbpa2*, and *cbpb1*), *chymotrypsin* (*ctrb*), and *chymotrypsin-like elastases* (*cel2a* and *cel3b*), all involved in protein digestion and absorption (Table 9 and Fig. S5), and pancreatic secretion (Table 4 and Fig. S2). The pancreatic secretion pathway was significantly bidirectionally perturbed only in the VH10P30 group, and several pancreatic amylases, proteases, and lipases were included only in the VH10P30 DEG list (Table 4 and Table S4), such as *alpha-amylase* (*amy*), *bile salt-activated lipase* (fragment) (*cel*), and *trypsin-2 (fragment)* (*try2*). On the other hand, an overall downregulation of *collagens* (*cra1b*, *cola1*, *co4a1*, *coia1*, *co1a2*, and *coha1*) in protein digestion and absorption (Table 9 and Fig. S5) was evident in the DI for both treatment groups.

Both PC and DI had a relatively low number of DEGs in comparing VH10P30 to CV as the negative control. In this comparison, a total of 20 (9 upregulated and 11 downregulated) DEGs were found in PC (Table S6), while 284 (175 upregulated and 109 downregulated) DEGs were found in DI (Table S7). Functional enrichment analysis found no significant differences in these comparisons, so we focused more on the comparisons using the CF group as a control, finding them more

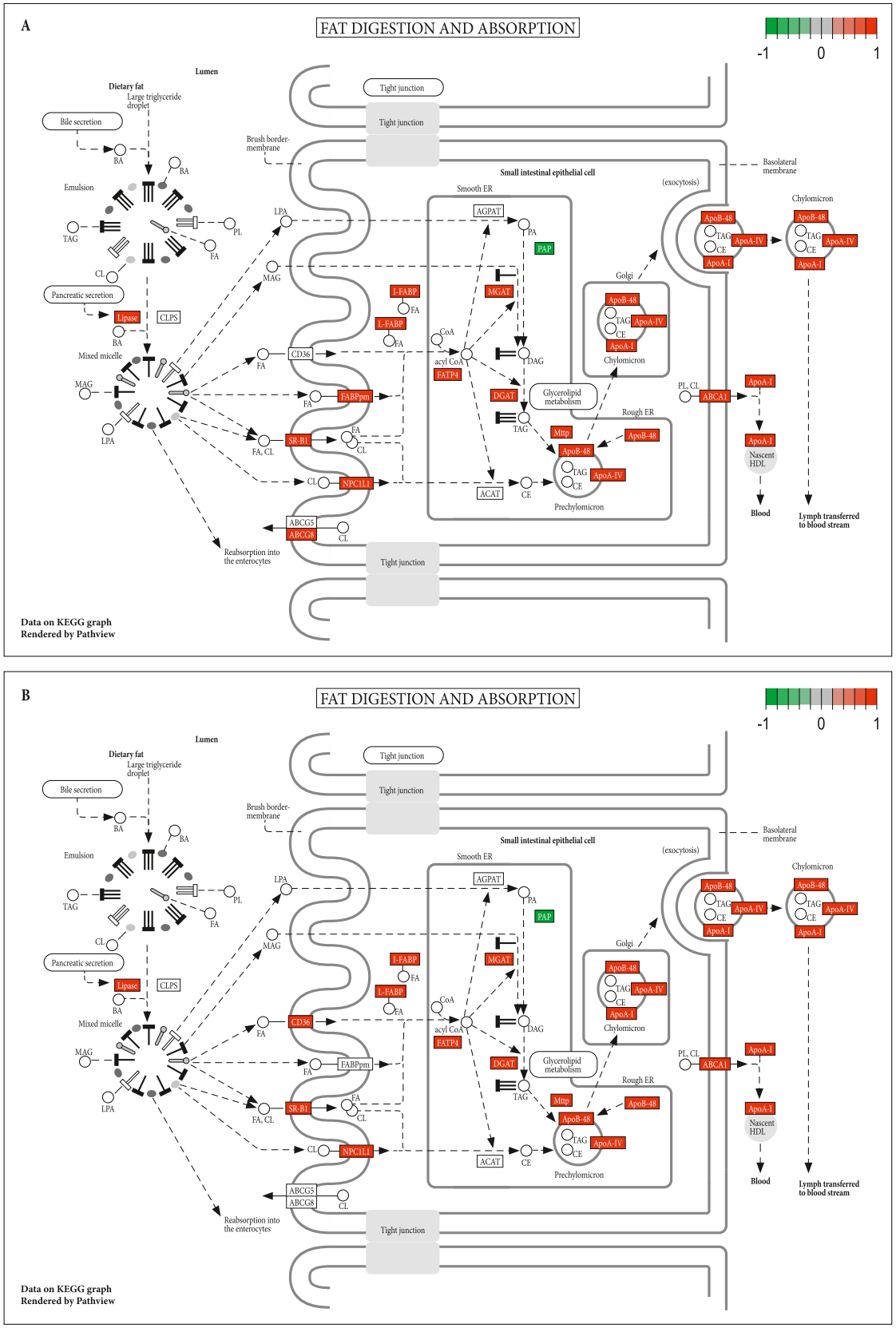

Fig. 4. Fat digestion and absorption pathway. (**A**) Visualisation of differentially expressed genes (DEGs) in the KEGG fat digestion and absorption pathway in the distal intestine of subadult European seabass in the VH10P30 vs. CF group (FDR < 0.05). (**B**) Visualisation of DEGs in the KEGG fat digestion and absorption pathway in the distal intestine of subadult European seabass in the CV vs. CF group (FDR < 0.05). Red indicates upregulated DEGs and green indicates downregulated DEGs. (For interpretation of the references to colour in this figure legend, the reader is referred to the web version of this article.)

Table 6
DEGs in the distal intestine identified in the KEGG fat digestion and absorption pathway.

Gene symbol	VH10P30 vs. CF logFC	padj	CV vs. CF logFC	padj	UNIPROT/ SWISSPROT description
apob	6.13	0.0000	2.40	0.0004	*Apolipoprotein B-100*
dgat2	4.44	0.0019	2.52	0.0008	*Diacylglycerol O-acyltransferase 2*
apoa1	4.21	0.0017	3.93	0.0031	*Apolipoprotein A-I*
cel	4.11	0.0001			*Bile salt-activated lipase (Fragment)*
scrb1	4.00	0.0000	3.23	0.0003	*Scavenger receptor class B member 1*
pg12b	3.76	0.0040	4.06	0.0014	*Group XIIB secretory phospholipase A2-like protein*
apoa4	3.30	0.0078	7.54	0.0000	*Apolipoprotein A-IV*
npcl1	3.01	0.0000	2.81	0.0001	*NPC1-like intracellular cholesterol transporter 1*
mog2a	2.96	0.0000	2.61	0.0000	*2-acylglycerol O-acyltransferase 2-A*
fabpi	2.74	0.0330	3.74	0.0019	*Fatty acid-binding protein, intestinal*
fabpl	2.66	0.0014	3.58	0.0000	*Fatty acid-binding protein, liver-type*
mtp	2.51	0.0004	3.31	0.0000	*Microsomal triglyceride transfer protein*
s27a4	2.41	0.0012	2.95	0.0000	*Long-chain fatty acid transport protein 4*
abca1	1.68	0.0025	1.76	0.0003	*Phospholipid-transporting ATPase ABCA1*
abcg8	1.51	0.0292			*ATP-binding cassette sub-family G member 8*
aatm	1.25	0.0291			*Aspartate aminotransferase, mitochondrial*
dgat1	0.94	0.0117	1.42	0.0141	*Diacylglycerol O-acyltransferase 1*
plpp2	−1.61	0.0000	−1.92	0.0000	*Phospholipid phosphatase 2*
cd36			3.85	0.0266	*Platelet glycoprotein 4*

DEGs are ordered by log2-fold change (logFC) value (from largest to smallest) in the VH10P30 vs. CF comparison, and if the same DEG was present in the CV vs. CF comparison, it is listed in the next column along with the associated p-adjusted value (padj). At the end of the table, DEGs that were present only in the comparison between CV and CF are listed, again in decreasing logFC order. DEGs were identified with a Benjamini-Hochberg false discovery rate (FDR) < 0.05.

informative on a systemic level. However, it is important to note that DEGs that we highlighted as different between the VH10P30 group and the CV group are also present in this analysis (namely *cbpa1*, *cbpa2*, *cbpb1*, *cel2a*, *cel3b*, *amy*, *cel*, and *try2*).

3.2. PC and DI tissue morphology and ultrastructure

3.2.1. Pyloric caeca

In the CF group, enterocytes of the PC showed normal morphology with elongated microvilli, numerous heterolysosomes and multivesicular bodies, indicating active absorption and digestion of the endocytosed particles (Fig. 6A). Individual intraepithelial lymphocytes were rarely visible (Fig. 6A, insert). Goblet cells were moderately large and contained either electron-lucent finely granulated mucin granules or electron-lucent and denser granules, indicating variable mucin content (Fig. 6B, C). The lamina propria showed normal morphology with a moderate number of well-formed collagen fibres and abundant finely granulated ground substance, corresponding to the loose connective tissue of this layer. The endothelial cells of the small capillaries of the lamina propria contained numerous pinocytotic vesicles (Fig. 6D). Electron-lucent lipid droplets of varying size were common around the capillaries in the lamina propria (Fig. 6E).

In the VH10P30 group, PC enterocytes also had normal cell morphology but contained numerous small subapical vesicles and accumulations of mitochondria with an electron-lucent matrix. Unusually large Golgi apparatus with prominent cisternae were the rule rather than the exception (Fig. 6F). Discharge of small multivesicular bodies were often detected (Fig. 6G). The goblet cells appeared somewhat larger than in the CF group and contained both electron-lucent and electron-dense mucin granules. Usually, a single large structure without granularity was observed in the cytoplasm, indicating recent mucus excretion rather than the coalescence of several small granules (Fig. 6H). Occasionally, these vacuoles contained small multilamellar structures (Fig. 6H, insert).

Dramatic changes were observed in the enterocytes of PC in the CV group compared to the other two groups. The microvilli appeared slightly shorter than in the PC of the other two groups, while the enterocytes had a foamy appearance due to numerous vacuoles of different sizes. Moderate lymphocyte infiltration was often seen in the expanded intercellular spaces (Fig. 6I). Vacuoles were more numerous in the central to basal part of the cells and appeared to be empty or containing highly electron-lucent content. Intercellular space was enlarged along the entire baso-apical axis and often contained fluid, i.e., exudate due to inflammation (Fig. 6J). Intraepithelial lymphocyte infiltration was more pronounced in the basal part near the basement membrane, where other immune cells, most likely macrophages, were also seen (Fig. 6K).

3.2.2. Distal intestine

In the CF group, DI enterocytes showed normal morphology, with well-developed microvilli, numerous heterolyzosomes, and large multivesicular bodies (Fig. 7A). Similar to the PC, goblet cells were moderately large and contained either electron-lucent or a combination of electron-lucent and electron-dense granules (Fig. 7B, C). Occasionally, goblet cells contained a single large vacuole, indicating recent mucus shedding (Fig. 7C). The endothelial cells of the capillaries of the lamina propria contained numerous pinocytotic vesicles, indicating marked absorption and transport of nutrients. In some cases, osmophilic and electron-dense inclusions, possibly lipid droplets, were seen in the cytoplasm of the endothelial cells (Fig. 7D, E). Rare rodlet cells with prominent cortex and variable number of rods could be observed infiltrating the lamina epithelialis (Fig. 7F).

In the VH10P30 group, DI enterocytes also showed normal morphology with well-developed microvilli, although the epithelium occasionally appeared oedematous, with a slightly expanded intracellular space and somewhat more infiltrating rodlet cells than in the CF group (Fig. 7G). Nevertheless, most intestinal villi appeared normal with distinct cellular junctions and numerous subapical absorptive vesicles and multivesicular bodies (Fig. 7G, insert). Goblet cells were large and elongated and contained both electron-lucent and denser granules (Fig. 7H). In the lamina propria, the endothelial cells of capillaries contained numerous pinocytotic vesicles, similar to those found in the CF group (Fig. 7I). Occasionally, eosinophilic granule cells (EGCs) could be seen near the capillaries infiltrating the connective tissue of the lamina propria, which contained larger amounts of collagen fibres, indicating some degree of fibrosis (Fig. 7J). Deeper in the lamina propria and closer to the submucosa, a more pronounced infiltration of EGCs was seen, sometimes surrounded by small electron-lucent lipid droplets (Fig. 7K, L). Dense bundles of formed collagen fibres were often surrounded by thin and extended cytoplasmic projections (telopods) indicative of subepithelial or stromal telocytes (Fig. 7L). An incidental finding in a single specimen from the VH10P30 group (not used for transcriptome sequencing), was a mild infection with the myxozoan *Kudoa* (*Sphaerosospora*) *dicentrarchi* detected in the muscularis externa (Fig. 7M).

In the CV group, DI enterocytes showed normal morphology with well-developed microvilli, numerous subapical heterolyzosomes and absorptive vesicles, and distinct cellular junctions (Fig. 7N). However,

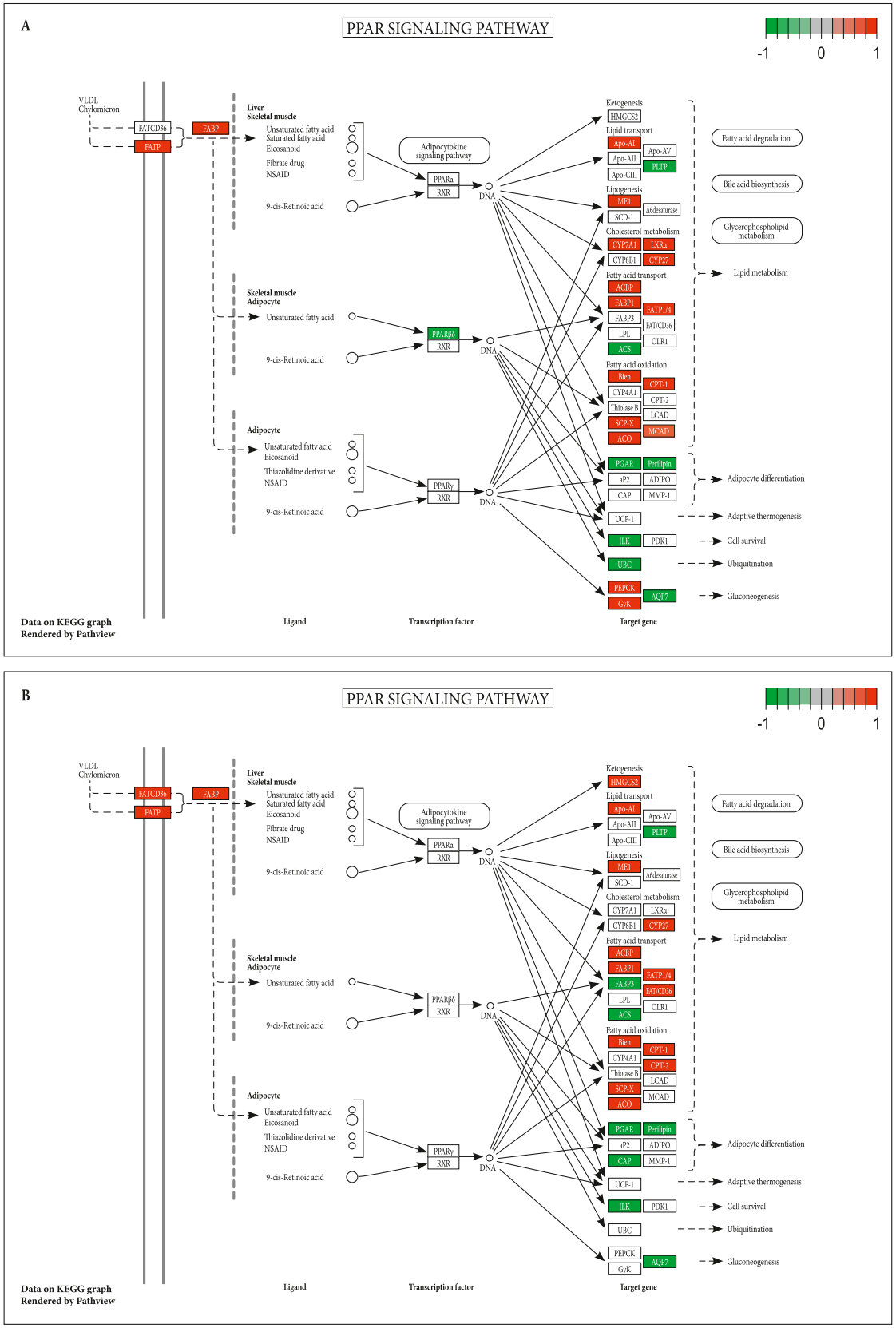

Fig. 5. PPAR signalling pathway. (**A**) Visualisation of differentially expressed genes (DEGs) in the KEGG PPAR signalling pathway in the distal intestine of subadult European seabass comparing the VH10P30 vs. CF group (FDR < 0.05). (**B**) Visualisation of DEGs in the KEGG PPAR signalling pathway in the distal intestine of subadult European seabass in the CV vs. CF group (FDR < 0.05). Red indicates upregulated DEGs and green indicates downregulated DEGs. (For interpretation of the references to colour in this figure legend, the reader is referred to the web version of this article.)

Table 7
DEGs in the distal intestine identified in the KEGG PPAR signalling pathway.

Gene symbol	VH10P30 vs. CF logFC	padj	CV vs. CF logFC	padj	UNIPROT/SWISSPROT description
cp7a1	5.54	0.0240			*Cytochrome P450 7A1*
apoa1	4.21	0.0017	3.93	0.0031	*Apolipoprotein A-I*
pckgm	3.06	0.0001			*Phosphoenolpyruvate carboxykinase [GTP], mitochondrial*
fabpi	2.74	0.0330	3.74	0.0019	*Fatty acid-binding protein, intestinal*
fabpl	2.66	0.0014	3.58	0.0000	*Fatty acid-binding protein, liver-type*
s27a4	2.41	0.0012	2.95	0.0000	*Long-chain fatty acid transport protein 4*
glpk	2.28	0.0285			*Glycerol kinase*
maox	2.04	0.0099	3.17	0.0000	*NADP-dependent malic enzyme*
scp2	1.98	0.0001	2.15	0.0000	*Sterol carrier protein 2*
cp27a	1.73	0.0008	1.41	0.0071	*Sterol 26-hydroxylase, mitochondrial*
acbp	1.58	0.0004	1.49	0.0007	*Acyl-CoA-binding protein*
acox3	1.55	0.0000	1.63	0.0000	*Peroxisomal acyl-coenzyme A oxidase 3*
cpt1a	1.48	0.0000	1.24	0.0000	*Carnitine O-palmitoyltransferase 1, liver isoform*
s27a2	1.39	0.0006	1.57	0.0001	*Long-chain fatty acid transport protein 2*
nr1h3	0.98	0.0090			*Oxysterols receptor LXR-alpha*
echp	0.86	0.0189	0.77	0.0327	*Peroxisomal bifunctional enzyme*
acadm	0.56	0.0303			*Medium-chain specific acyl-CoA dehydrogenase, mitochondrial*
ppard	−1.01	0.0408			*Peroxisome proliferator-activated receptor delta*
plin2	−1.70	0.0073	−1.99	0.0012	*Perilipin-2*
pltp	−1.75	0.0175	−3.22	0.0000	*Phospholipid transfer protein*
angl4	−1.80	0.0004	−2.12	0.0000	*Angiopoietin-related protein 4*
ilk	−2.15	0.0003	−1.90	0.0013	*Integrin-linked protein kinase*
aqp7	−2.23	0.0085	−2.65	0.0015	*Aquaporin-7*
acsl3	−2.24	0.0111	−2.74	0.0014	*Fatty acid CoA ligase Acsl3*
ubiqp	−5.23	0.0145			*Polyubiquitin (Fragment)*
fabp7			4.11	0.0398	*Fatty acid-binding protein, brain*
cd36			3.85	0.0266	*Platelet glycoprotein 4*
hmcs1			3.33	0.0493	*Hydroxymethylglutaryl-CoA synthase, cytoplasmic*
cpt2			1.61	0.0301	*Carnitine O-palmitoyltransferase 2, mitochondrial*
fabp4			−1.48	0.0245	*Fatty acid-binding protein, adipocyte*
srbs1			−2.88	0.0072	*Sorbin and SH3 domain-containing protein 1*

DEGs are ordered by log2-fold change (logFC) value (from largest to smallest) in the VH10P30 vs. CF comparison, and if the same DEG was present in the CV vs. CF comparison, it is listed in the next column along with the associated p-adjusted value (padj). At the end of the table, DEGs that were present only in the comparison between CV and CF are listed, again in decreasing logFC order. DEGs were identified with a Benjamini-Hochberg false discovery rate (FDR) < 0.05.

over a large area of the intestine, a thin protein layer was seen over the microvilli, most likely containing fibrin/fibrinogen deposits (Fig. 7N, insert). The goblet cells were elongated and almost exclusively contained electron-lucent mucus granules. Basally, moderate to extensive lymphocyte infiltration was present in the lamina epithelialis near the basement membrane (Fig. 7O). In the lamina propria, large deposits of nascent collagen fibres were present in the lamina propria, often around

Table 8
DEGs in the distal intestine identified in the KEGG vitamin digestion and absorption pathway.

Gene symbol	VH10P30 vs. CF logFC	padj	CV vs. CF logFC	padj	UNIPROT/SWISSPROT description
apob	6.13	0.0000	2.40	0.0004	*Apolipoprotein B-100*
plb1	5.18	0.0008	4.07	0.0087	*Phospholipase B1, membrane-associated*
ret2	4.34	0.0058	5.02	0.0009	*Retinol-binding protein 2*
apoa1	4.21	0.0017	3.93	0.0031	*Apolipoprotein A-I*
scrb1	4.00	0.0000	3.23	0.0003	*Scavenger receptor class B member 1*
apoa4	3.30	0.0078	7.54	0.0000	*Apolipoprotein A-IV*
s19a3	3.06	0.0000	3.35	0.0000	*Thiamine transporter 2*
btd	2.17	0.0035	2.00	0.0067	*Biotinidase*
s23a1	1.82	0.0006	2.35	0.0000	*Solute carrier family 23 member 1*
pcft	1.59	0.0220	1.68	0.0123	*Proton-coupled folate transporter*
cubn	−8.03	0.0000	−5.51	0.0000	*Cubilin*
sc5a6			1.64	0.0002	*Sodium-dependent multivitamin transporter*
s5a3a			1.62	0.0110	*Solute carrier family 52, riboflavin transporter, member 3-A*

DEGs are ordered by log2-fold change (logFC) value (from largest to smallest) in the VH10P30 vs. CF comparison, and if the same DEG was present in the CV vs. CF comparison, it is listed in the next column along with the associated p-adjusted value (padj). At the end of the table, DEGs that were present only in the comparison between CV and CF are listed, again in decreasing logFC order. DEGs were identified with a Benjamini-Hochberg false discovery rate (FDR) < 0.05.

small blood vessels and surrounded by thin cytoplasmic projections (telopods) of telocytes. Distally, from the cell body, telopods often contained larger number of podomeres and podoms. The connective tissue of the lamina propria was conspicuously infiltrated by various populations of immune cells, including lymphocytes, rare plasma cells, and EGCs (Fig. 7P), some of which were in the process of degranulation (Fig. 7Q). Electron-lucent lipid droplets of varying sizes were rarely seen (Fig. 7R).

4. Discussion

The fish intestine has numerous functions beyond digestion and nutrient absorption, including water and electrolyte balance, nutrient sensing, pathogen recognition, and regulation of the intestinal microbiome (Calduch-Giner et al., 2016; Martin et al., 2016). This functional diversity has been confirmed with histological and molecular approaches commonly used in nutrition and immunity to study fish species (Betancor et al., 2017; Calduch-Giner et al., 2012; Kokou et al., 2019; Liu et al., 2022). Compared to studies on the intestinal microbiome (Antonopoulou et al., 2019; Bruni et al., 2018; Legrand et al., 2020; Martinez-Guryn et al., 2018; Mikołajczak et al., 2020; Moroni et al., 2021; Wang et al., 2018; Zarantoniello et al., 2020), transcriptomic studies related to alternative protein or lipid sources in fish diets are relatively rare. In addition to the liver, transcriptome profiling of different parts of the intestine has proven to be a useful tool for evaluating the impact of alternative dietary sources (Caballero-Solares et al., 2018; Fan et al., 2021; Morais et al., 2012; Zhao et al., 2020). Previous studies reported different transcriptomic responses between European seabass half-families in terms of protein and ATP synthesis in the liver (Geay et al., 2011) or compared the transcriptomic response of different fish organs to dietary changes (Tacchi et al., 2012; Ye et al., 2023), but we believe this is the first comparison of two intestinal parts at the transcriptomic level in European seabass nutritional research.

Table 9
DEGs in the distal intestine identified in the KEGG protein digestion and absorption pathway.

Gene symbol	VH10P30 vs. CF logFC	padj	CV vs. CF logFC	padj	UNIPROT/ SWISSPROT description
mep1b	5.66	0.0004	2.58	0.0036	*Meprin A subunit beta*
cbpa2	5.12	0.0003			*Carboxypeptidase A2*
cel2a	4.84	0.0000			*Chymotrypsin-like elastase family member 2 A*
cel3b	4.61	0.0000			*Chymotrypsin-like elastase family member 3B*
ctrb	4.59	0.0000			*Chymotrypsin B*
cbpb1	4.57	0.0001			*Carboxypeptidase B*
try2	4.00	0.0000			*Trypsin-2 (Fragment)*
cbpa1	3.93	0.0013			*Carboxypeptidase A1*
s15a1	3.93	0.0000	2.91	0.0022	*Solute carrier family 15 member 1*
ace2	3.89	0.0000	2.84	0.0000	*Angiotensin-converting enzyme 2*
nep	3.35	0.0000	2.24	0.0000	*Neprilysin*
mep1a	3.10	0.0000	2.05	0.0000	*Meprin A subunit alpha*
s6a19	2.93	0.0008	2.24	0.0123	*Sodium-dependent neutral amino acid transporter B(0)AT1*
ylat1	2.09	0.0001			*Y + L amino acid transporter 1*
at233	1.93	0.0001	−1.80	0.0017	*Sodium/potassium-transporting ATPase subunit beta-233*
slc31	1.56	0.0132	1.85	0.0022	*Neutral and basic amino acid transport protein rBAT*
mot10	1.50	0.0030			*Monocarboxylate transporter 10*
dpp4	1.26	0.0465	1.65	0.0054	*Dipeptidyl peptidase 4*
lat2	0.61	0.0174	1.01	0.0000	*Large neutral amino acids transporter small subunit 2*
cra1b	−1.91	0.0041	−3.01	0.0000	*Collagen alpha-1 (XXVII) chain B*
co6a1	−1.93	0.0024			*Collagen alpha-1(VI) chain*
cola1	−1.97	0.0087	−2.16	0.0032	*Collagen alpha-1(XXI) chain*
at1a1	−2.02	0.0000	−1.78	0.0001	*Sodium/potassium-transporting ATPase subunit alpha-1*
co4a1	−2.09	0.0003	−1.90	0.0009	*Collagen alpha-1(IV) chain*
nac2	−2.46	0.0011			*Sodium/calcium exchanger 2*
coia1	−2.47	0.0037	−3.45	0.0000	*Collagen alpha-1(XVIII) chain*
co1a2	−2.72	0.0005	−2.21	0.0046	*Collagen alpha-2(I) chain*
coha1	−2.72	0.0034	−3.70	0.0001	*Collagen alpha-1(XVII) chain*
bat1	−4.79	0.0266			*b(0,+)-type amino acid transporter 1*
trp3			2.65	0.0007	*Trypsinogen-like protein 3*
xpp2			2.15	0.0173	*Xaa-Pro aminopeptidase 2*
4f2			1.30	0.0022	*4F2 cell-surface antigen heavy chain*
cola1			1.49	0.0082	*Collagen alpha-1(XXI) chain*
coca1			−2.45	0.0014	*Collagen alpha-1(XII) chain*
co6a3			−2.80	0.0000	*Collagen alpha-3(VI) chain*
nac3			−2.94	0.0001	*Sodium/calcium exchanger 3*
ylat2			−2.96	0.0003	*Y + L amino acid transporter 2*
coda1			−3.66	0.0319	*Collagen alpha-1(XIII) chain*

DEGs are ordered by log2-fold change (logFC) value (from largest to smallest) in the VH10P30 vs. CF comparison, and if the same DEG was present in the CV vs. CF comparison, it is listed in the next column along with the associated p-adjusted value (padj). At the end of the table, DEGs that were present only in the comparison between CV and CF are listed, again in decreasing logFC order. DEGs were identified with a Benjamini-Hochberg false discovery rate (FDR) < 0.05.

The nutrigenomic approach used here revealed a profound effect of a plant-based diet (CV) and a diet including plants, black soldier fly meal, and poultry by-product (VH10P30) on the digestive system (protein, fat, and vitamin digestion and absorption), endocrine system (PPAR signalling pathway), and signalling molecules and interactions (neuroactive ligand-receptor interaction). In some respects, the VH10P30 and CV diets were more similar in terms of metabolic transcriptional profile than might have been expected based on the previously published histomorphology (Lepen Pleić et al., 2022) and ultrastructural features of the distal intestine and in particular the pyloric caeca, as presented here. Observed supranuclear vacuolisation of enterocytes in the CV group, abundant lymphocyte infiltration in the lamina epithelialis and the lamina propria, and detachment of the lamina epithelialis from the lamina propria, were significantly improved by the addition of black soldier fly and poultry by-product meals in the VH10P30 group (Lepen Pleić et al., 2022), which was confirmed using TEM.

4.1. Difference in PC and DI transcriptomes as a reflection of functional specialisation

A somewhat unexpected finding was the striking difference in transcriptomic response of the distal intestine (DI) and pyloric caeca (PC) within the same treatment, for both the VH10P30 and CV diets. In both instances, DI showed higher sensitivity to the introduced dietary changes and many DEGs related to digestion and absorption, while only a handful of DEGs were detected in PC. These differences in gene expression between intestinal segments may be an indicator of functional specialisation along the intestine. The DI plays an important role in nutrient absorption, and changes in gene expression patterns may reflect the need for enhanced digestion and absorption of proteins, fats, and vitamins in response to the introduced dietary change. Previous research in European seabass reported an overrepresentation of molecular and cellular functions related to feed digestion, nutrient uptake and transport in the anterior and middle part of the intestinal tract, while the initiation and establishment of immune defence mechanisms are particularly relevant in the DI (Calduch-Giner et al., 2016). It was somewhat surprising that the immune response in the CV group was not evident at the transcriptomic level in the DI. However, it must be taken into account that even when comparing the same intestinal segment between studies, the exact location of sampling can vary greatly, e.g., one study stated that the DI was sampled as a segment that included the rectum (Calduch-Giner et al., 2016), while in the present study the sample was taken from the middle of the DI, which might make our section functionally somewhere in between the middle intestine and the DI from their study. This could also be the reason why the immune response was not captured in the transcriptomes of the CV group. Meanwhile, only a small number of DEGs in PC play a role in immune response, while the ultrastructural study clearly showed elements of inflammation and/or tissue repair.

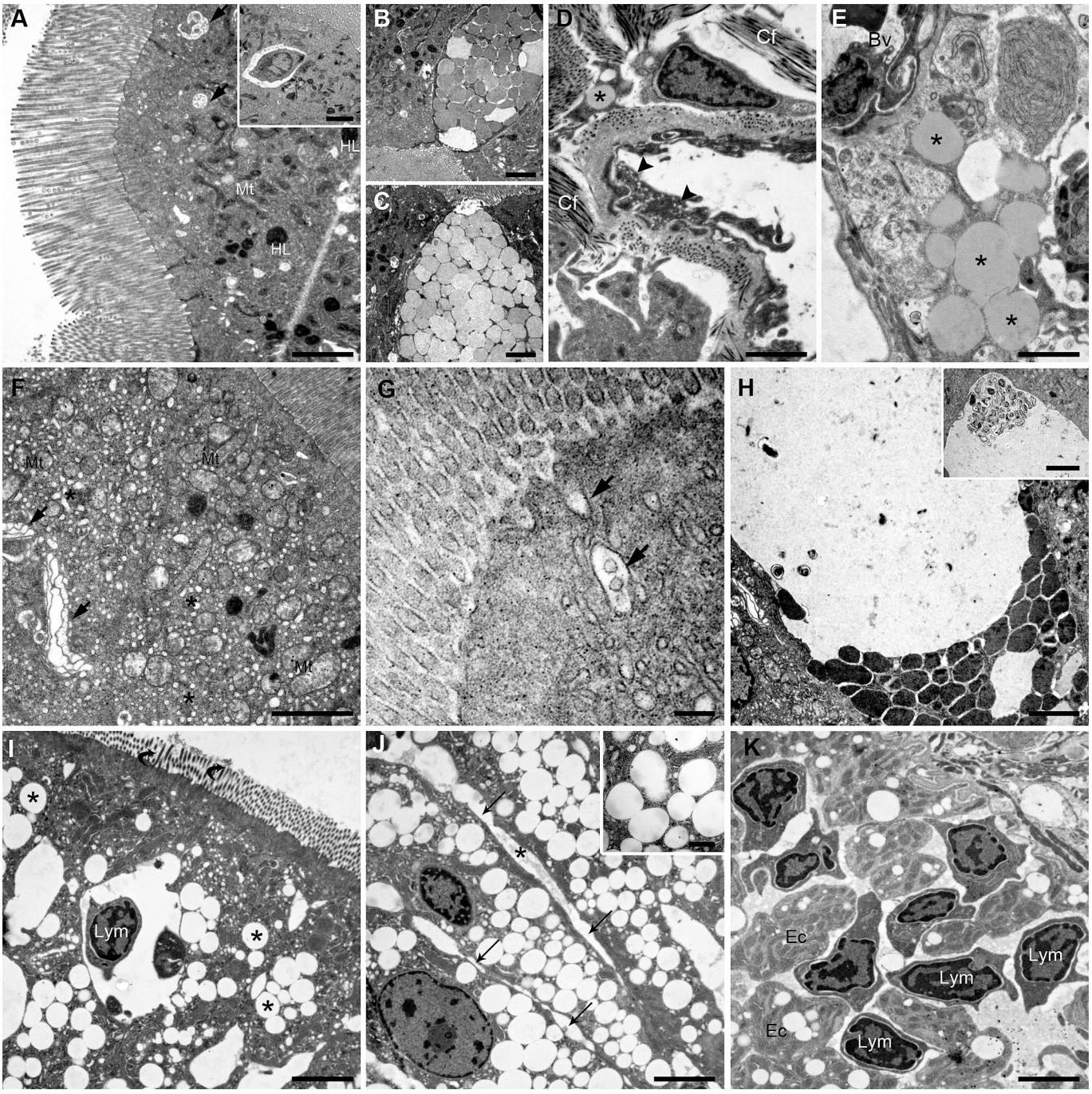

Fig. 6. Pyloric caeca TEM. Representative TEM microscopic images of the pyloric caeca of fish fed commercial fishmeal-based feed (CF) (**A-E**), plant-based feed with added black soldier fly meal and poultry by-product meal (VH10P30) (**F—H**) and plant-based feed (CV) (**I—K**). (**A**) Overview of enterocytes showing normal morphology, well preserved and elongated microvilli and normal junctional complexes. The cytoplasm is filled with darkly stained heterolysosomes (HL) and numerous mitochondria (Mt). Several multivesicular bodies of varying size are seen subapically (short arrows). Occasionally some intraepithelial lymphocytes are seen (insert). (**B—C**) Goblet cells with mucus granules of varying electronic density and granularity. (**D**) Small blood vessel in the lamina propria with numerous pinocytotic vesicles within the endothelial cells (arrowheads). Numerous bundles of mature collagen fibres (Cf) surround the blood vessel with a single electron-lucent lipid droplet (asterisk). (**E**) Deeper in the lamina propria, abundant lipid droplets (asterisks) of various sizes are seen around small blood vessels (Bv). (**F**) Apical part of the enterocyte with numerous mitochondria (Mt), numerous small absorptive vacuoles (asterisks) and prominent Golgi apparatus with large cisternae (short arrows). (**G**) Outflow of small multivesicular bodies (short arrows). (**H**) Goblet cells with large central vacuole, most likely due to recent mucus excretion, and numerous basally located electron-dense granules. (**I**) Overview of enterocytes with extensive vacuolisation (asterisk) and cell damage. The intercellular spaces are dilated and occasionally populated with intraepithelial lymphocytes (Lym). Shortened microvilli are seen on the apical membrane (curved arrows). (**J**) Basal parts of enterocytes with dilated intercellular spaces (arrows) filled with electron-lucent fluid (asterisks). Numerous vacuoles appear to be mostly empty or contain highly electron-lucent contents (inset). (**K**) Cross-section through the basal part of the lamina epithelials showing numerous infiltrating lymphocytes (Lym) and possibly other immune cells between highly vacuolised enterocytes (Ec).

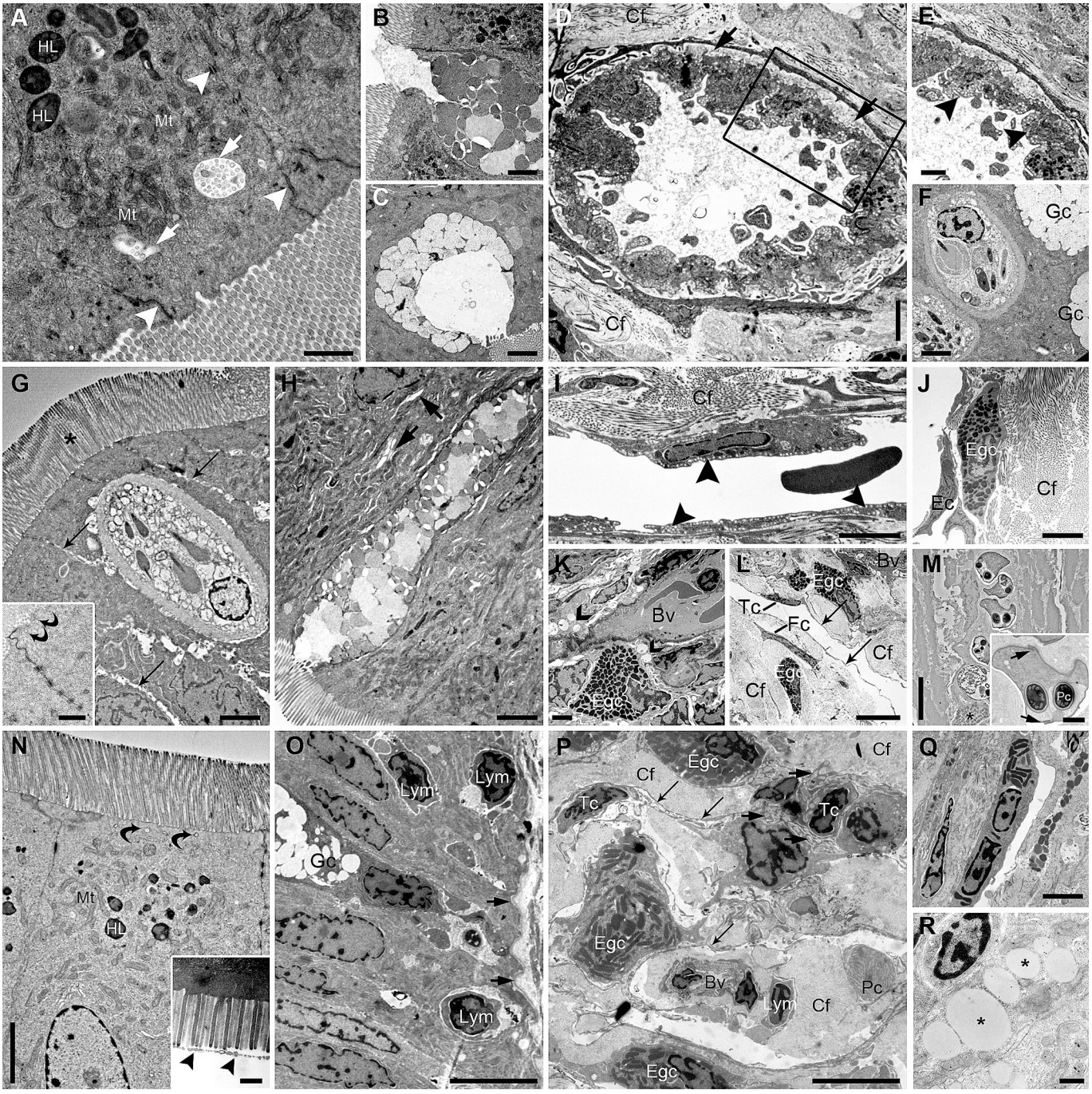

(caption on next page)

Fig. 7. Distal intestine TEM. Representative TEM microscopic images of the distal intestine of fish fed commercial feed (CF) (**A-F**), plant-based feed with added black soldier fly meal and poultry by-product meal (VH10P30) (**G-M**) and plant-based feed (CV) (**N-R**). (**A**) Overview of enterocytes with normal morphology and normal, conspicuous junctional complexes (arrowheads). The cytoplasm is filled with large, darkly stained heterolysosomes (HL) and numerous mitochondria (Mt). Several multivesicular bodies of different sizes can be seen subapically (short arrows). (**B-C**) Goblet cells during mucus secretion with mucus granules of different electron density and granularity. (**D**) Small blood vessel in the lamina propria with numerous pinocytotic vesicles within the endothelial cells lying on the thick basement membrane (short arrows). Bundles of mature collagen fibres (Cf) and abundant finely granular ground substance surround the blood vessel. (**E**) Higher magnification of the area marked with a rectangle in panel **D**. It shows innumerable pinocytotic vesicles (arrowheads) and highly electron dense inclusions within the endothelial cells, most likely lipid droplets. (**F**) Intraepithelial rodlet cells adjacent to two goblet cells (Gc) with distinct cellular cortex and varying numbers of rods. (**G**) Overview of enterocytes with normal microvillar morphology (asterisk). The intercellular spaces are slightly dilated but do not contain fluid. A single intraepithelial rodlet cell with highly granulated cytoplasm can be seen. Inset: Formation of subapical absorptive vesicles (curved arrows). Note the normal and well-developed junctional complexes (tight junction, adherens junction and desmosomes). (**H**) Large, elongated goblet cell with mucus granules of varying electron density. Adjacent enterocytes contain large Golgi apparatus with prominent cisternae (short arrows). (**I**) Small blood vessel in the lamina propria with endothelial cells filled with pinocytotic vesicles (arrowheads). The surrounding connective tissue contains a greater amount of mature collagen fibres (Cf). (**J**) Deeper in the lamina propria, more collagen fibres (Cf) are present. A single eosinophilic granule cell (Egc) is seen near the endothelial cell (Ec), indicating recent extravasation. (**K**) Detail of the lamina propria showing several small electron-lucent lipid droplets (empty arrows) surrounding a small blood vessel and a single eosinophilic granule cell (Egc) with numerous cytoplasmic granules. (**L**) Deeper region of the lamina propria with abundant deposits of mature collagen fibres (Cf) surrounding a small blood vessel (Bv) and bordered by thin telopods (thin arrows) of telocytes (Tc). Several recently extravasated eosinophilic granules cells (Egc) and a single elongated fibrocyte (Fc) can be seen. (**M**) Myxospores of *Kudoa* (*Sphaerospora*) *dicentrarchi* between smooth muscle cells of the muscularis externa and a single eosinophilic granule cell (Egc). Inset: Detail of a myxospore with its wall connected along suture lines (short arrows) and with two polar capsules (Pc) with polar filaments. (**N**) Overview of enterocytes with normal morphology, well-developed microvilli and normal junctional complexes. The cytoplasm is filled with large, darkly stained heterolysosomes (HL) and numerous mitochondria (Mt). Several subapical absorptive vesicles (curved arrows) are formed. A thin proteinaceous film covers the microvilli (insert, arrowheads). (**O**) Basal part of the lamina epithelials near the basement membrane (short arrows) with several intraepithelial lymphocytes (Lym). A single goblet cell (Gc) with basal nucleus surrounded by endoplasmic reticulum contains highly electron-lucent mucus granules. (**P**) Lamina propria filled with large bundles of mature and nascent collagen fibres (Cf) surrounded by thin telopods (thin arrows) of several telocytes (Tc). The telopods contain numerous podomeres with large podoms (short arrows). A mixed population of infiltrating cells can be seen, including eosinophilic granule cells (Egc), lymphocytes (Lym) and a single plasma cell (Pc) near a small blood vessel (Bv). Deeper in the lamina propria, occasionally degranulated Egc can be seen. (**R**) Large electron-lucent lipid droplets (asterisks).

4.2. Reduced inflammation and/or tissue repair

In a previous study of the extent of adaptability of European seabass to total replacement of a fish-based diet with a plant-based diet (Geay et al., 2011), an interesting finding was the downregulation of genes involved in the innate immune response and the pro-inflammatory pathway, which could be compared to the absence of an immune response at the transcriptomic level presented here, supported by ultrastructural evidence of a resolving inflammation and tissue repair process. The absence of an inflammatory response has been linked to the high expression of *fabp7*, a fatty acid binding protein recently recognised as critical for regulating the inflammatory response in astrocytes (Killoy et al., 2020), and to the downregulation of *C-reactive protein* (*crp*), an acute-phase protein synthesised by hepatocytes, in plant-based diet groups (Geay et al., 2011). The lack of immune response may be due in part to a defect in the membrane properties of the plant diet groups, supported by the downregulation of a large number of genes related to cell communication, including cell surface receptor binding proteins and/or cell adhesion receptors involved in the immune response in our study. Alternatively, as suggested by Estruch et al. (Estruch et al., 2018), who fed gilthead seabream (*Sparus aurata*) a plant protein-based diet, long periods of feeding such diets could lead to depressive or suppressive effects on immune mechanisms and other pathways demanding continuous energy supply. Finally, it should be taken into account that the fish were partially fed and sampled in winter, when lower sea temperatures could have dampened the immune response.

In addition to a significant upregulation of *fabp7*, the CV group also showed several other significantly perturbed KEGG signalling pathways related to cell communication, such as ECM-receptor interaction and cell adhesion molecules (CAMs) pathways (Fig. S6 and Fig. S7). The fact that many of the genes in these two pathways were downregulated (e.g., *collagen*, *laminin*, *fibronectin*) suggests not only that the inflammation due to anti-nutrients in the plant-based diet was declining, but also that the intestinal tissue had entered a remodelling phase following the healing process. Such an assumption is further supported by the upregulation of occluding and cadherin, major proteins of tight junctions (Furuse et al., 1994) and adherens junctions and desmosomes (Priest et al., 2019), respectively, possibly indicating the establishment of novel junctional complexes between enterocytes of recently repaired epithelium. In all fish, enterocytes presented with similar cytoplasmic electron density, normal tight junction complexes and normal microvillar morphology, though this was somewhat shorter in the CV group, and this is in line with previously reported ultrastructural observations in European seabass fed novel feed formulations (Torrecillas et al., 2023). While there was a mild to moderate infiltration of leukocytes in the intestines in the CF and VH10P30 groups, considerably higher numbers of infiltrating leukocytes, particularly intraepithelial lymphocytes were seen in the intestine of the CV group. This might be associated with upregulation of *il16* in PC of the VH10P30 and CV groups, stimulating a migratory response in CD4+ lymphocytes, monocytes, and eosinophils, and primes CD4+ T-cells for Il-2 and Il-15 responsiveness. In turn, Il-2 and Il-15 play important roles in the homeostasis of innate and adaptive immunity (Yang and Lundqvist, 2020). Another upregulated gene detected only in the PC of the CV group was *i17el*, which is predicted to enable interleukin-17 receptor activity. As there is lack of systematic immune response and none of the overrepresented KEGG pathways are related to immunity, the evidence at the transcriptomic level is not compelling in this direction.

Lastly, regarding the finding of the histozoic *Kudoa* (*Sphaerospora*) *dicentrarchi*, we speculate that the presence of this myxozoan parasite did not influence the inflammatory repertoire in the VH10P30 group. Although this parasite can cause systemic infections and a chronic cumulative effect on the host as a consequence of a progressive increase of infection rate with age (Sitjà-Bobadilla and Alvarez-Pellitero, 1993), documented pathological effects of this parasite on cultured European seabass are rare (Fioravanti et al., 2004). Furthermore, it was found in the muscularis externa and associated only with a few eosinophilic granule cells, while most of the inflammatory infiltrate was seen in the mucosal layer.

4.3. Similarity or dissimilarity between transcriptomes of the CV and VH10P30 groups

Greater transcriptome changes detected in the CV vs. VH10P30 group in both PC and DI analyses could be indicative of lower overall fitness of fish in the CV group. Lower overall fitness of fish has previously been associated with the magnitude of transcriptomic changes detected in fish fed terrestrial animal and/or plant protein diets (Dam et al., 2020; Król et al., 2016). A study of yellowtail kingfish (*Seriola lalandi*) concluded that the diets that showed the least changes at the

transcriptomic level compared to a fishmeal-based diet were the most promising for the industry (Dam et al., 2020), and the results aligned well with previous research on the apparent digestibility of the tested raw materials used in their diets (Dam et al., 2019). Interestingly, one of the ingredients that scored positively in their research was poultry by-product meal at 30%, as included in the VH10P30 diet in this study. Thanks to our previous extensive study of VH10P30 and CV diets using a multidisciplinary approach (Lepen Pleić et al., 2022), we believe that the changes detected at the transcriptome level should be interpreted in combination with TEM and the quality of the final product published previously, with emphasis on the proximal composition and fatty acid profiles of the fillets.

The fatty acid profile of the fillet is the result of complex metabolic processes, mainly involving the intestine and liver, which occur between feed intake, digestion, and lipid deposition in the fillet (Bakke et al., 2010). Although the process of lipid absorption in fish has been observed in the proximal regions of the intestine and pyloric caeca (Denstadli et al., 2004; Hernandez-Blazquez et al., 2006), it likely depends on lipid class, chain length, and degree of saturation. Short- and medium-chain fatty acids are thought to be absorbed rapidly in the most proximal/anterior part of the intestine. In contrast, saturated long-chain fatty acids, due to their high hydrophobicity and lower micellar solubility, may not reach the brush border as easily and may not be absorbed as readily as fatty acids with a similar chain length but lower degree of saturation (Bakke et al., 2010; Morais et al., 2005a; Morais et al., 2005b; Oxley et al., 2007). This could explain why major adaptations occurred at the transcriptomic level in DI in our study. The observed upregulation of apolipoproteins in our study has been reported in numerous studies exploring the effects of low-fishmeal or plant-based diets in various fish species (Dam et al., 2020; Geay et al., 2011; Leaver et al., 2008b; Leduc et al., 2018; Tacchi et al., 2012) and starvation studies (Martin et al., 2010; Qian et al., 2016). However, there were some differences between the VH10P30 and CV diets. *Apob*, the major component of low-density lipoproteins (LDL) and chylomicrons involved in the transport of cholesterol and lipids from the liver to other tissues, had a higher logFC in the VH10P30 group (Table 6), in combination with the upregulation of *bile salt-activated lipase* (*cel*), which was upregulated only in the VH10P30 diet and is considered the major lipase in marine fish (Bakke et al., 2010). On the other hand, *apoa1*, which is the major protein component of high-density lipoprotein (HDL) and participates in the reverse transport of cholesterol from tissues to the liver for excretion and acts as a cofactor for lecithin cholesterol acyltransferase (Lcat), had a higher logFC in the CV group.

Stimulation of cholesterol synthesis and transport was previously found to be an important response in the liver of European seabass fed a plant-based diet, and it was hypothesised that the reduced dietary cholesterol content associated with low fishmeal content would likely result in reduced cellular cholesterol content in the fish (Geay et al., 2011). In both the VH10P30 and CV groups, there was ample evidence of cholesterol synthesis and transport, although some of the overexpressed genes were not shared between the diets. For example, in the CV group, *cytoplasmic hydroxymethylglutaryl-CoA synthase* (*hmcs1*) was upregulated (Table 7), and its role is catalysing the condensation of acetyl-CoA with acetoacetyl-CoA to form HMG-CoA, which is converted by HMG-CoA reductase (Hmgcr) to mevalonate, a precursor for cholesterol synthesis. In the VH10P30 group, *cytochrome P450 family 7 subfamily A member 1* (*cp7a1*) was upregulated (Table 7); this is a cytochrome P450 monooxygenase that is involved in the metabolism of endogenous cholesterol and its oxygenated derivatives and also functions as a critical regulatory enzyme of bile acid biosynthesis and cholesterol homeostasis. Another gene that was upregulated only in the VH10P30 group was the *ATP binding cassette subfamily G member 8* (*abcg8*) (Table 6), which plays an essential role in the selective transport of the dietary cholesterol in and out of the enterocytes and in the selective sterol excretion by the liver into bile. It appears that each of the two experimental groups dealt with the decreased dietary cholesterol in a specific manner, and it is possible that the addition of black soldier fly meal and poultry by-product meal reduced the pressure to synthesise as much endogenous cholesterol as in the CV group, as seen by the disturbances to the steroid biosynthesis pathway (Fig. S8). Another explanation could be that the VH10P30 group metabolised cholesterol more efficiently, as shown in the map of PPAR pathways (Fig. 5). The *peroxisome proliferator-activated receptor delta* (*ppard* or *pparδ*) was downregulated in the VH10P30 group, although the PPAR signalling pathway was differentially perturbed in both the CV and VH10P30 groups (Fig. 5, Table S4 and Table S5). PPARs belong to the nuclear hormone receptor superfamily and are ligand-activated transcription factors involved in translating the effects of fat soluble factors such as hormones, vitamins, fatty acids and various drugs to the level of gene expression (Gervois et al., 2000). Pparα increases cellular fatty acid uptake, esterification and trafficking and regulates genes of lipoprotein metabolism. Pparδ stimulates lipid and glucose utilisation by improving mitochondrial function and fatty acid desaturation pathways. In contrast, Pparγ promotes fatty acid uptake, triglyceride formation and storage in lipid droplets, improving insulin sensitivity and glucose metabolism (Montaigne et al., 2021). The relationship between PPARs and fatty acid binding protein (Fabp) activity is complex and may be context-dependent (Hotamisligil and Bernlohr, 2015). Fabps are a family of small, highly conserved, cytoplasmic proteins that bind long-chain fatty acids and other hydrophobic ligands. It is generally considered that the role of Fabps include fatty acid uptake, transport, and metabolism (UniProt Consortium, 2017). Studies in fish have shown that the expression of *fabps* responds to dietary fatty acids (Torstensen et al., 2009; Xu et al., 2017). The *liver fatty acid binding protein* (*fabpl* or *fabp1*), which was significantly upregulated in the VH10P30 and CV groups, is a soluble 14 kDa protein found in the cytoplasm of hepatocytes and to a lesser extent in the nucleus and outer mitochondrial membrane. *Fabpl* is also found in many other tissues, such as enterocytes, and it plays a central role in β-oxidation, both through fatty acid trafficking and Pparα mediated regulation of gene expression. There are interspecies differences in the presence or absence of Fabpl in different organs and in its content (Wang et al., 2015). The *intestinal fatty acid binding protein* (*fabpi* or *fabp2*), also significantly upregulated in both the VH10P30 and CV groups, is involved in the uptake, intracellular metabolism and transport of long-chain fatty acids. Fabpi can transport lipids from the intestinal lumen to the enterocytes and bind excess fatty acids to maintain a constant fatty acid pool in the epithelium. As a lipid chaperone, Fabpi can also transport lipophilic drugs to facilitate targeted transport. Recently, it has been suggested that it may serve as a clinical biomarker, as Fabpi is released into the bloodstream when the integrity of the intestinal epithelium is disrupted (Huang et al., 2022). Interestingly, *cd36*, a gene that was significantly upregulated only in the CV group, has been found to play a previously unsuspected role in maintaining the integrity of the epithelial barrier. This role appears to be separate from that of lipid uptake and metabolism, but may suggest that Cd36 dysfunction in the intestine could increase susceptibility to inflammation as a result of abnormalities in intestinal fat processing (Cifarelli and Abumrad, 2018). Global deletion of Cd36 in mice results in abnormal remodelling of the extracellular matrix in the proximal small intestine and a leaky epithelial barrier with neutrophil infiltration and inflammation (Cifarelli et al., 2017).

There were many similarities in terms of fat digestion and absorption in the VH10P30 and CV groups. When considering similarities between the two experimental diets, it is also important to consider their composition, i.e., both diets contained 66% non-fish lipids and 34% fish oil, which were inverse to the proportions in the CF diet (Lepen Pleić et al., 2022). Therefore, it is not surprising that the European seabass response was similar in these two groups, although there were some differences in the composition of alternative ingredients. However, the decrease of only 15–18% in EPA and DHA compared to the CF group (Lepen Pleić et al., 2022) confirmed the positive evaluation of the nutritional quality of all fish groups in this study.

Furthermore, the chemical composition of the fillet muscle showed no differences between the three diet groups presented here (Lepen Pleić et al., 2022). The intestine in general has a very high cell turnover rate and consequently a high level of protein synthesis and protein degradation. Although insulin mediates carbohydrate metabolism in fish, this role is minimal compared to its role in protein metabolism, as it stimulates amino acid uptake and protein synthesis, decreases protein turnover, and inhibits gluconeogenesis from amino acids. In addition, amino acids in fish are more potent secretagogues of insulin than glucose. Insulin also increases lipogenesis and inhibits lipolysis (Caruso and Sheridan, 2011). Interpreting the effect of the insulin secretion pathway in the CV group (Fig. S3) is complex since certain genes were downregulated while others were upregulated, but one possible explanation may be that perturbation of insulin secretion pathway was connected to altered protein metabolism, as opposed to carbohydrate metabolism. There were undoubtedly differences in the protein digestion pathway in the VH10P30 and CV groups, as evidenced by the upregulation of *carboxypeptidases* (*cbpa1, cbpa2*, and *cbpb1*), *chymotrypsin* (*ctrb*), and *chymotrypsin-like elastases* (*cel2a* and *cel3b*) in the VH10P30 group only. Carboxypeptidases are peptidases that sequentially remove the most C-terminal residues of a peptide until either the peptide is completely degraded or a point is reached that prevents further degradation (Hegemann, 2022). Cbpa1 and Cbpa2 have a similar function, though Cbpa2 has a preference for bulkier C-terminal residues, while Cbpa1 has little or no action with aspartic acid, glutamic acid, arginine, lysine or proline amino acid and preferentially releases C-terminal lysine or arginine amino acid. A number of carboxypeptidases upregulated in this study show a specific adaptation that occurred in the VH10P30 group but was absent in the CV group. It is generally recognised that the higher the gene expression, the higher the expected enzyme activity. However, the number of gene transcripts does not always correlate with the amount of protein transcribed, as mRNA levels may be regulated post-transcriptionally and/or translationally, or there may even be protein degradation/turnover. It is hypothesised that ~40% of the variation in protein concentration can be explained by knowledge of mRNA abundances (Vogel and Marcotte, 2012), and it is important to understand the limitations of interpreting transcriptomic data.

Previously mapped functional specialisation of seabass intestinal segments found that genes related to vitamin B12 absorption were among the highest ranked DEGs in DI, including *cubn* (Calduch-Giner et al., 2016), which was downregulated in this study in both the VH10P30 and CV groups. Cubn is an endocytic receptor that plays a role in lipoprotein, vitamin, and iron metabolism by facilitating the uptake of these substances. Downregulation of *cubn* could have a potential impact on the absorption of vitamin B12 and other nutrients that rely on the cubilin-mediated pathway. However, further research would be needed to investigate the consequences of this downregulation on the overall nutrient status of seabass and the compensatory mechanisms employed in the distal intestine for nutrient absorption.

5. Conclusions

The research presented here demonstrated a strong transcriptomic response of subadult European seabass after a 22-week trial comparing a plant-based diet (CV) and a diet consisting of plant protein, black soldier fly meal, and poultry by-product (VH10P30) to a fishmeal-based diet (CF) as the control. The distal intestine was more sensitive to these dietary changes than the pyloric caeca, and DEGs mainly affected digestion and absorption of proteins, fats, and vitamins in both experimental diets containing plants. The overall transcriptomic changes were greater in the CV group than in the VH10P30 group and included a greater number of perturbed metabolic and signalling pathways. In contrast to the transcriptomic results, the ultrastructural findings indicated a decrease of inflammation and/or evidence of tissue repair in the CV group, particularly in the pyloric caeca. Since the nutritional quality of all fish groups in this study was previously evaluated positively, with a decrease of only 15–18% in EPA and DHA, changes detected at the transcriptome level can be interpreted as evidence of the adaptability of European seabass and its ability to efficiently utilise various nutrients. Finally, the present study confirms that the performance of subadult European seabass on a plant-based diet is improved at the molecular level by the addition of poultry by-products and black soldier fly meal.

Supplementary data to this article can be found online at https://doi.org/10.1016/j.aquaculture.2024.741385.

CRediT authorship contribution statement

Željka Trumbić: Writing – review & editing, Formal analysis. **Jerko Hrabar:** Writing – original draft, Visualization, Investigation. **Ivana Lepen-Pleić:** Writing – review & editing, Investigation. **Tanja Šegvić-Bubić:** Writing – review & editing, Project administration, Investigation. **Elisavet Kaitetzidou:** Writing – review & editing, Investigation. **Emilio Tibaldi:** Writing – review & editing, Methodology, Funding acquisition. **Ivana Bočina:** Writing – original draft, Visualization, Investigation, Funding acquisition, Formal analysis. **Leon Grubišić:** Writing – review & editing, Project administration, Investigation. **Elena Sarropoulou:** Writing – review & editing, Supervision, Resources, Formal analysis.

Declaration of competing interest

The authors declare that they have no competing interests.

Data availability

All data supporting our findings are included in the manuscript and its supplementary information. RNA-Seq raw data were submitted to the NCBI Sequence Read Archive (SRA) under BioProject accession number PRJNA956721.

Acknowledgments

The authors are thankful to all members of the Laboratory of Aquaculture in Split for their help during the feeding trial and sampling and graphic designer Sandra Garber (design and programming studio 'Kombinat') for preparing the KEGG figures in Adobe InDesign.

This work benefited from access to IMBBC-HCMR, an EMBRC-GR and EMBRC-ERIC operator. Financial support was provided by EMBRC-ERIC and the European Marine Research Network (EuroMarine) through their joint 2020 call targeting early career researchers, Interreg AdriAquaNet (Project ID 10045161), and SustainAqua (funded by NextGenerationEU-National Recovery and Resilience Plan 2021-2026). This work also benefited from access to the Cluster Isabella at the University of Zagreb Computing Centre (SRCE) (https://www.srce.unizg.hr/en/advanced-computing).

References

Abdel-Latif, H.M.R., Abdel-Tawwab, M., Khalil, R.H., Metwally, A.A., Shakweer, M.S., Ghetas, H.A., Khallaf, M.A., 2021. Black soldier fly (*Hermetia illucens*) larvae meal in diets of European seabass: effects on antioxidative capacity, non-specific immunity, transcriptomic responses, and resistance to the challenge with *vibrio alginolyticus*. Fish Shellfish Immunol. 111, 111–118. https://doi.org/10.1016/j.fsi.2021.01.013.

Abdel-Latif, H.M.R., Abdel-Daim, M.M., Shukry, M., Nowosad, J., Kucharczyk, D., 2022. Benefits and applications of *Moringa oleifera* as a plant protein source in aquafeed: a review. Aquaculture 547, 737369. https://doi.org/10.1016/J.AQUACULTURE.2021.737369.

Abdel-Tawwab, M., Khalil, R.H., Metwally, A.A., Shakweer, M.S., Khallaf, M.A., Abdel-Latif, H.M.R., 2020. Effects of black soldier fly (*Hermetia illucens* L.) larvae meal on growth performance, organs-somatic indices, body composition, and hemato-biochemical variables of European sea bass, *Dicentrarchus labrax*. Aquaculture 522, 735136. https://doi.org/10.1016/j.aquaculture.2020.735136.

Alasalvar, C., Taylor, K.D.A., Zubcov, E., Shahidi, F., Alexis, M., 2002. Differentiation of cultured and wild sea bass (*Dicentrarchus labrax*): total lipid content, fatty acid and

trace mineral composition. Food Chem. 79, 145–150. https://doi.org/10.1016/S0308-8146(02)00122-X.
Antonopoulou, E., Nikouli, E., Piccolo, G., Gasco, L., Gai, F., Chatzifotis, S., Mente, E., Kormas, K.A., 2019. Reshaping gut bacterial communities after dietary *Tenebrio molitor* larvae meal supplementation in three fish species. Aquaculture 503, 628–635. https://doi.org/10.1016/j.aquaculture.2018.12.013.
Bakke, A.M., Glover, C., Krogdahl, Å., 2010. Feeding, digestion and absorption of nutrients. Fish Physiol. 57–110.
Betancor, M.B., Li, K., Sprague, M., Bardal, T., Sayanova, O., Usher, S., Han, L., Masøval, K., Torrissen, O., Napier, J.A., Tocher, D.R., Olsen, R.E., 2017. An oil containing EPA and DHA from transgenic *Camelina sativa* to replace marine fish oil in feeds for Atlantic salmon (*Salmo salar* L.): effects on intestinal transcriptome, histology, tissue fatty acid profiles and plasma biochemistry. PLoS ONE 12, 1–29. https://doi.org/10.1371/journal.pone.0175415.
Bolger, A.M., Lohse, M., Usadel, B., 2014. Trimmomatic: a flexible trimmer for Illumina sequence data. Bioinformatics 30, 2114–2120. https://doi.org/10.1093/bioinformatics/btu170.
Bonaldo, A., Roem, A.J., Fagioli, P., Pecchini, A., Cipollini, I., Gatta, P.P., 2008. Influence of dietary levels of soybean meal on the performance and gut histology of gilthead sea bream (*Sparus aurata* L.) and European sea bass (*Dicentrarchus labrax* L.). Aquac. Res. 39, 970–978. https://doi.org/10.1111/j.1365-2109.2008.01958.x.
Bonvini, E., Bonaldo, A., Mandrioli, L., Sirri, R., Dondi, F., Bianco, C., Fontanillas, R., Mongile, F., Gatta, P.P., Parma, L., 2018. Effects of feeding low fishmeal diets with increasing soybean meal levels on growth, gut histology and plasma biochemistry of sea bass. Animal 12, 923–930. https://doi.org/10.1017/S1751731117002683.
Boukid, F., Riudavets, J., Del Arco, L., Castellari, M., 2021. Impact of diets including agro-industrial by-products on the fatty acid and sterol profiles of larvae biomass from *Ephestia kuehniella, Tenebrio molitor* and *Hermetia illucens*. Insects 12. https://doi.org/10.3390/insects12080672.
Bruni, L., Pastorelli, R., Viti, C., Gasco, L., Parisi, G., 2018. Characterisation of the intestinal microbial communities of rainbow trout (*Oncorhynchus mykiss*) fed with *Hermetia illucens* (black soldier fly) partially defatted larva meal as partial dietary protein source. Aquaculture 487, 56–63. https://doi.org/10.1016/j.aquaculture.2018.01.006.
Caballero-Solares, A., Xue, X., Parrish, C.C., Foroutani, M.B., Taylor, R.G., Rise, M.L., 2018. Changes in the liver transcriptome of farmed Atlantic salmon (*Salmo salar*) fed experimental diets based on terrestrial alternatives to fish meal and fish oil. BMC Genomics 19, 1–26. https://doi.org/10.1186/s12864-018-5188-6.
Calder, P.C., 2014. Very long chain omega-3 (n-3) fatty acids and human health. Eur. J. Lipid Sci. Technol. 116, 1280–1300. https://doi.org/10.1002/ejlt.201400025.
Calduch-Giner, J.A., Sitjà-Bobadilla, A., Davey, G.C., Cairns, M.T., Kaushik, S., Pérez-Sánchez, J., 2012. Dietary vegetable oils do not alter the intestine transcriptome of gilthead sea bream (*Sparus aurata*), but modulate the transcriptomic response to infection with *Enteromyxum leei*. BMC Genomics 13, 1–13. https://doi.org/10.1186/1471-2164-13-470.
Calduch-Giner, J.A., Sitjà-Bobadilla, A., Pérez-Sánchez, J., 2016. Gene expression profiling reveals functional specialization along the intestinal tract of a carnivorous teleostean fish (*Dicentrarchus labrax*). Front. Physiol. 7, 1–17. https://doi.org/10.3389/fphys.2016.00359.
Camacho, C., Coulouris, G., Avagyan, V., Ma, N., Papadopoulos, J., Bealer, K., Madden, T.L., 2009. BLAST+: architecture and applications. BMC Bioinformatics 10, 1–9. https://doi.org/10.1186/1471-2105-10-421.
Campos, I., Matos, E., Aragão, C., Pintado, M., Valente, L.M.P., 2018. Apparent digestibility coefficients of processed agro-food by-products in European seabass (*Dicentrarchus labrax*) juveniles. Aquac. Nutr. 24, 1274–1286. https://doi.org/10.1111/anu.12665.
Campos, I., Matos, E., Maia, M.R.G., Marques, A., Valente, L.M.P., 2019. Partial and total replacement of fish oil by poultry fat in diets for European seabass (*Dicentrarchus labrax*) juveniles: effects on nutrient utilization, growth performance, tissue composition and lipid metabolism. Aquaculture 502, 107–120. https://doi.org/10.1016/j.aquaculture.2018.12.004.
Cantalapiedra, C.P., Hernandez-Plaza, A., Letunic, I., Bork, P., Huerta-Cepas, J., 2021. eggNOG-mapper v2: functional annotation, orthology assignments, and domain prediction at the metagenomic scale. Mol. Biol. Evol. 38, 5825–5829. https://doi.org/10.1093/molbev/msab293.
Caruso, M.A., Sheridan, M.A., 2011. Pancreas. In: Farrell, A.P. (Ed.), Encyclopedia of Fish Physiology: From Genome to Environment. Elsevier, pp. 1276–1283.
Cifarelli, V., Abumrad, N.A., 2018. Intestinal CD36 and other key proteins of lipid utilization: role in absorption and gut homeostasis. Compr. Physiol. 8 (2), 493–507. https://doi.org/10.1002/cphy.c170026.
Cifarelli, V., Ivanov, S., Xie, Y., Son, N.H., Saunders, B.T., Pietka, T.A., Shew, T.M., Yoshino, J., Sundaresan, S., Davidson, N.O., Goldberg, I.J., Gelman, A.E., Zinselmeyer, B.H., Randolph, G.J., Abumrad, N.A., 2017. CD36 deficiency impairs the small intestinal barrier and induces subclinical inflammation in mice. Cell. Mol. Gastroenterol. Hepatol. 3 (1), 82–98. https://doi.org/10.1016/j.jcmgh.2016.09.001.
Corley, S.M., Troy, N.M., Bosco, A., Wilkins, M.R., 2019. QuantSeq. 3′ sequencing combined with Salmon provides a fast, reliable approach for high throughput RNA expression analysis. Sci. Rep. 9, 1–15. https://doi.org/10.1038/s41598-019-55434-x.
Dam, C.T.M., Elizur, A., Ventura, T., Salini, M., Smullen, R., Pirozzi, I., Booth, M., 2019. Apparent digestibility of raw materials by yellowtail kingfish (*Seriola lalandi*). Aquaculture 511, 734233. https://doi.org/10.1016/j.aquaculture.2019.734233.
Dam, C.T.M., Ventura, T., Booth, M., Pirozzi, I., Salini, M., Smullen, R., Elizur, A., 2020. Intestinal transcriptome analysis highlights key differentially expressed genes involved in nutrient metabolism and digestion in yellowtail kingfish (*Seriola lalandi*) fed terrestrial animal and plant proteins. Genes 11, 1–17. https://doi.org/10.3390/genes11060621.
Denstadli, V., Vegusdal, A., Krogdahl, Å., Bakke-Mckellep, A.M., Berge, G.M., Holm, H., Hillestad, M., Ruyter, B., 2004. Lipid absorption in different segments of the gastrointestinal tract of Atlantic salmon (*Salmo salar* L.). Aquaculture 240, 385–398. https://doi.org/10.1016/j.aquaculture.2004.06.030.
Dobin, A., Davis, C.A., Schlesinger, F., Drenkow, J., Zaleski, C., Jha, S., Batut, P., Chaisson, M., Gingeras, T.R., 2013. STAR: ultrafast universal RNA-seq aligner. Bioinformatics 29, 15–21. https://doi.org/10.1093/BIOINFORMATICS/BTS635.
EFSA, 2010. Scientific opinion on dietary reference values for fats, including saturated fatty acids, polyunsaturated fatty acids, monounsaturated fatty acids, trans fatty acids, and cholesterol. EFSA J. 8, 1461. https://doi.org/10.2903/j.efsa.2010.1461.
Estruch, G., Collado, M.C., Monge-Ortiz, R., Tomas-Vidal, A., Jover-Cerda, M., Penaranda, D.S., Martinez, G.P., Martinez-Llorens, S., 2018. Long-term feeding with high plant protein based diets in gilthead seabream (*Sparus aurata*, L.) leads to changes in the inflammatory and immune related gene expression at intestinal level. BMC Vet. Res. 14 https://doi.org/10.1186/s12917-018-1626-6.
Fan, J.Q., Lu, K.C., Chen, G.L., Li, B.B., Song, F., Chen, Y.H., 2021. Transcriptome analysis of the influence of high plant protein based diet on *Trachinotus ovatus* liver. Fish Shellfish Immunol. 119, 339–346. https://doi.org/10.1016/J.FSI.2021.10.013.
FAO, 2018. Food and Agriculture Organization of the United Nations. The State of World Fisheries and Aquaculture 2018 - Meeting the Sustainable Development Goals, Rome.
FAO/WHO, 2008. Interim summary of conclusions and dietary recommendations on Total fat & Fatty Acids. In: Joint FAO/WHO Expert Consultation on Fats and Fatty Acids in Human Nutrition, Geneva. WHO, pp. 1–14.
Fioravanti, M.L., Caffara, M., Florio, D., Gustinelli, A., Marcer, F., 2004. *Sphaerospora dicentrarchi* and *S. Testicularis* (Myxozoa: Sphaerosporidae) in farmed European seabass (*Dicentrarchus labrax*) from Italy. Folia Parasitol. 51 (2–3), 208–210. https://doi.org/10.14411/fp.2004.024.
Furuse, M., Itoh, M., Hirase, T., Nagafuchi, A., Yonemura, S., Tsukita, S., Tsukita, S., 1994. Direct association of occludin with ZO-1 and its possible involvement in the localization of occludin at tight junctions. J. Cell Biol. 127 (6), 1617–1626. https://doi.org/10.1083/jcb.127.6.1617.
Galkanda-Arachchige, H.S.C., Wilson, A.E., Davis, D.A., 2020. Success of fishmeal replacement through poultry by-product meal in aquaculture feed formulations: a meta-analysis. Rev. Aquac. 12, 1624–1636. https://doi.org/10.1111/raq.12401.
Gatlin, D.M., Barrows, F.T., Brown, P., Dabrowski, K., Gaylord, T.G., Hardy, R.W., Herman, E., Hu, G., Krogdahl, Å., Nelson, R., Overturf, K., Rust, M., Sealey, W., Skonberg, D., Souza, E.J., Stone, D., Wilson, R., Wurtele, E., 2007. Expanding the utilization of sustainable plant products in aquafeeds: a review. Aquac. Res. 38, 551–579. https://doi.org/10.1111/j.1365-2109.2007.01704.x.
Geay, F., Ferraresso, S., Zambonino-Infante, J.L., Bargelloni, L., Quentel, C., Vandeputte, M., Kaushik, S., Cahu, C.L., Mazurais, D., 2011. Effects of the total replacement of fish-based diet with plant-based diet on the hepatic transcriptome of two European sea bass (*Dicentrarchus labrax*) half-sibfamilies showing different growth rates with the plant-based diet. BMC Genomics 12, 1–18. https://doi.org/10.1186/1471-2164-12-522.
Gentleman, R.C., Carey, V.J., Bates, D.M., Bolstad, B., Dettling, M., Dudoit, S., Ellis, B., Gautier, L., Ge, Y., Gentry, J., Hornik, K., Hothorn, T., Huber, W., Iacus, S., Irizarry, R., Leisch, F., Li, C., Maechler, M., Rossini, A.J., Sawitzki, G., Smith, C., Smyth, G., Tierney, L., Yang, J.Y.H., Zhang, J., 2004. Bioconductor: open software development for computational biology and bioinformatics. Genome Biol. 5.
Gervois, P., Torra, I.P., Fruchart, J.-C., Staels, B., 2000. Regulation of lipid and lipoprotein metabolism by PPAR activators. Clin. Chem. Lab. Med. 38, 3–11. https://doi.org/10.1067/mjd.2001.113718.
Glencross, B.D., Baily, J., Berntssen, M.H.G., Hardy, R., MacKenzie, S., Tocher, D.R., 2020. Risk assessment of the use of alternative animal and plant raw material resources in aquaculture feeds. Rev. Aquac. 12, 703–758. https://doi.org/10.1111/raq.12347.
Hegemann, J.D., 2022. Combined thermal and carboxypeptidase Y stability assays for probing the threaded fold of lasso peptides. In: Pyle, A.M., Christianson, D.W. (Eds.), Methods Enzymol, pp. 177–204.
Hernandez-Blazquez, F.J., Guerra, R.R., Kfoury, J.R., Bombonato, P.P., Cogliati, B., Silva, J.R.M.C.D., 2006. Fat absorptive processes in the intestine of the Antarctic fish *Notothenia coriiceps* (Richardson, 1844). Polar Biol. 29, 831–836. https://doi.org/10.1007/s00300-006-0121-x.
Hotamisligil, G.S., Bernlohr, D.A., 2015. Metabolic functions of FABPs–mechanisms and therapeutic implications. Nat. Rev. Endocrinol. 11 (10), 592–605. https://doi.org/10.1038/nrendo.2015.122.
Howe, K.L., Achuthan, P., Allen, J., Allen, J., Alvarez-Jarreta, J., Ridwan Amode, M., Armean, I.M., Azov, A.G., Bennett, R., Bhai, J., Billis, K., Boddu, S., Charkhchi, M., Cummins, C., da Rin Fioretto, L., Davidson, C., Dodiya, K., El Houdaigui, B., Fatima, R., Gall, A., Giron, C.G., Grego, T., Guijarro-Clarke, C., Haggerty, L., Hemrom, A., Hourlier, T., Izuogu, O.G., Juettemann, T., Kaikala, V., Kay, M., Lavidas, I., Le, T., Lemos, D., Martinez, J.G., Marugán, J.C., Maurel, T., McMahon, A.C., Mohanan, S., Moore, B., Muffato, M., Oheh, D.N., Paraschas, D., Parker, A., Parton, A., Prosovetskaia, I., Sakthivel, M.P., Abdul Salam, A.I., Schmitt, B.M., Schuilenburg, H., Sheppard, D., Steed, E., Szpak, M., Szuba, M., Taylor, K., Thormann, A., Threadgold, G., Walts, B., Winterbottom, A., Chakiachvili, M., Chaubal, A., de Silva, N., Flint, B., Frankish, A., Hunt, S.E., Ilsley, G.R., Langridge, N., Loveland, J.E., Martin, F.J., Mudge, J.M., Morales, J., Perry, E., Ruffier, M., Tate, J., Thybert, D., Trevanion, S.J., Cunningham, F., Yates, A.D., Zerbino, D.R., Flicek, P., 2021. Ensembl 2021. Nucleic Acids Res. 49, D884–D891. https://doi.org/10.1093/NAR/GKAA942.

Huang, X., Zhou, Y., Sun, Y., Wang, Q., 2022. Intestinal fatty acid binding protein: a rising therapeutic target in lipid metabolism. Prog. Lipid Res. 87, 101178 https://doi.org/10.1016/j.plipres.2022.101178.

Karapanagiotidis, I.T., Psofakis, P., Mente, E., Malandrakis, E., Golomazou, E., 2019. Effect of fishmeal replacement by poultry by-product meal on growth performance, proximate composition, digestive enzyme activity, haematological parameters and gene expression of gilthead seabream (*Sparus aurata*). Aquac. Nutr. 25, 3–14. https://doi.org/10.1111/anu.12824.

Kaushik, S.J., 2002. European sea bass, *Dicentrarchus labrax*. In: Webster, C.D., Lim, C. (Eds.), Nutrient Requirements and Feeding of Finfish for Aquaculture. CAB International, Wallingford, UK, pp. 28–39.

Kaushik, S.J., Covès, D., Dutto, G., Blanc, D., 2004. Almost total replacement of fish meal by plant protein sources in the diet of a marine teleost, the European seabass, *Dicentrarchus labrax*. Aquaculture 230, 391–404. https://doi.org/10.1016/S0044-8486(03)00422-8.

Killoy, K.M., Harlan, B.A., Pehar, M., Vargas, M.R., 2020. FABP7 upregulation induces a neurotoxic phenotype in astrocytes. Glia 68 (12), 2693–2704. https://doi.org/10.1002/glia.23879.

Kokou, F., Sasson, G., Friedman, J., Eyal, S., Ovadia, O., Harpaz, S., Cnaani, A., Mizrahi, I., 2019. Core gut microbial communities are maintained by beneficial interactions and strain variability in fish. Nat. Microbiol. 4, 2456–2465. https://doi.org/10.1038/s41564-019-0560-0.

Kopylova, E., Noé, L., Touzet, H., 2012. SortMeRNA: fast and accurate filtering of ribosomal RNAs in metatranscriptomic data. Bioinformatics 28, 3211–3217. https://doi.org/10.1093/BIOINFORMATICS/BTS611.

Król, E., Douglas, A., Tocher, D.R., Crampton, V.O., Speakman, J.R., Secombes, C.J., Martin, S.A.M., 2016. Differential responses of the gut transcriptome to plant protein diets in farmed Atlantic salmon. BMC Genomics 17, 1–16. https://doi.org/10.1186/s12864-016-2473-0.

Leaver, M.J., Bautista, J.M., Björnsson, B.T., Jönsson, E., Krey, G., Tocher, D.R., Torstensen, B.E., 2008a. Towards fish lipid nutrigenomics: current state and prospects for fin-fish aquaculture. Rev. Fish. Sci. 16, 71–92. https://doi.org/10.1080/10641260802325278.

Leaver, M.J., Villeneuve, L.A.N., Obach, A., Jensen, L., Bron, J.E., Tocher, D.R., Taggart, J.B., 2008b. Functional genomics reveals increases in cholesterol biosynthetic genes and highly unsaturated fatty acid biosynthesis after dietary substitution of fish oil with vegetable oils in Atlantic salmon (*Salmo salar*). BMC Genomics 9, 1–15. https://doi.org/10.1186/1471-2164-9-299.

Leduc, A., Zatylny-Gaudin, C., Robert, M., Corre, E., Corguille, G.L., Castel, H., Lefevre-Scelles, A., Fournier, V., Gisbert, E., Andree, K.B., Henry, J., 2018. Dietary aquaculture by-product hydrolysates: impact on the transcriptomic response of the intestinal mucosa of European seabass (*Dicentrarchus labrax*) fed low fish meal diets. BMC Genomics 19, 1–20. https://doi.org/10.1186/s12864-018-4780-0.

Legrand, T.P.R.A., Wynne, J.W., Weyrich, L.S., Oxley, A.P.A., 2020. A microbial sea of possibilities: current knowledge and prospects for an improved understanding of the fish microbiome. Rev. Aquac. 12, 1101–1134. https://doi.org/10.1111/raq.12375.

Lepen Pleić, I., Bušelić, I., Messina, M., Hrabar, J., Žuvić, L., Talijančić, I., Žužul, I., Pavelin, T., Anđelić, I., Pleadin, J., Puizina, J., Grubišić, L., Tibaldi, E., Šegvić-Bubić, T., 2022. A plant-based diet supplemented with *Hermetia illucens* alone or in combination with poultry by-product meal: one step closer to sustainable aquafeeds for European seabass. J. Anim. Sci. Biotechnol. 13, 1–22. https://doi.org/10.1186/S40104-022-00725-Z.

Li, B., Dewey, C.N., 2011. RSEM: accurate transcript quantification from RNA-Seq data with or without a reference genome. BMC Bioinformatics 12, 323. https://doi.org/10.1186/1471-2105-12-323.

Liu, Y., Yan, Y., Han, Z., Zheng, Y., Wang, X., Zhang, M., Li, H., Xu, J., Chen, X., Ding, Z., Cheng, H., 2022. Comparative effects of dietary soybean oil and fish oil on the growth performance, fatty acid composition and lipid metabolic signaling of grass carp, *Ctenopharyngodon idella*. Aquac. Rep. 22 https://doi.org/10.1016/J.AQREP.2021.101002.

Love, M.I., Huber, W., Anders, S., 2014. Moderated estimation of fold change and dispersion for RNA-seq data with DESeq2. Genome Biol. 15, 1–21. https://doi.org/10.1186/s13059-014-0550-8.

Luo, W., Brouwer, C., 2013. Pathview: an R/Bioconductor package for pathway-based data integration and visualization. Bioinformatics 29, 1830–1831. https://doi.org/10.1093/bioinformatics/btt285.

Luo, W., Friedman, M.S., Shedden, K., Hankenson, K.D., Woolf, P.J., 2009. GAGE: generally applicable gene set enrichment for pathway analysis. BMC Bioinformatics 10, 1–17. https://doi.org/10.1186/1471-2105-10-161.

Magalhães, R., Sánchez-López, A., Leal, R.S., Martínez-Llorens, S., Oliva-Teles, A., Peres, H., 2017. Black soldier fly (*Hermetia illucens*) pre-pupae meal as a fish meal replacement in diets for European seabass (*Dicentrarchus labrax*). Aquaculture 476, 79–85. https://doi.org/10.1016/j.aquaculture.2017.04.021.

Martin, S.A.M., Douglas, A., Houlihan, D.F., Secombes, C.J., 2010. Starvation alters the liver transcriptome of the innate immune response in Atlantic salmon (*Salmo salar*). BMC Genomics 11. https://doi.org/10.1186/1471-2164-11-418.

Martin, S.A.M., Dehler, C.E., Król, E., 2016. Transcriptomic responses in the fish intestine. Dev. Comp. Immunol. 64, 103–117. https://doi.org/10.1016/j.dci.2016.03.014.

Martinez-Guryn, K., Hubert, N., Frazier, K., Urlass, S., Musch, M.W., Ojeda, P., Pierre, J. F., Miyoshi, J., Sontag, T.J., Cham, C.M., Reardon, C.A., Leone, V., Chang, E.B., 2018. Small intestine microbiota regulate host digestive and absorptive adaptive responses to dietary lipids. Cell Host Microbe 23, 458–469.e455. https://doi.org/10.1016/j.chom.2018.03.011.

Mastoraki, M., Mollá Ferrándiz, P., Vardali, S.C., Kontodimas, D.C., Kotzamanis, Y.P., Gasco, L., Chatzifotis, S., Antonopoulou, E., 2020. A comparative study on the effect of fish meal substitution with three different insect meals on growth, body composition and metabolism of European sea bass (*Dicentrarchus labrax* L.). Aquaculture 528, 735511. https://doi.org/10.1016/j.aquaculture.2020.735511.

Mikołajczak, Z., Rawski, M., Mazurkiewicz, J., Kierończyk, B., Józefiak, D., 2020. The effect of hydrolyzed insect meals in sea trout fingerling (*Salmo trutta* m. *trutta*) diets on growth performance, microbiota and biochemical blood parameters. Animals 10, 1–20. https://doi.org/10.3390/ani10061031.

Moll, P., Ante, M., Seitz, A., Reda, T., 2014. QuantSeq 3′ mRNA sequencing for RNA quantification. Nat. Methods 11, i–iii. https://doi.org/10.1038/nmeth.f.376.

Montaigne, D., Butruille, L., Staels, B., 2021. PPAR control of metabolism and cardiovascular functions. Nat. Rev. Cardiol. 18, 809–823. https://doi.org/10.1038/s41569-021-00569-6.

Morais, S., Koven, W., Rønnestad, I., Teresa Dinis, M., Conceição, L.E.C., 2005a. Dietary protein:lipid ratio and lipid nature affects fatty acid absorption and metabolism in a teleost larva. Br. J. Nutr. 93, 813–820. https://doi.org/10.1079/bjn20051378.

Morais, S., Rojas-Garcia, C.R., Conceição, L.E.C., Rønnestad, I., 2005b. Digestion and absorption of a pure triacylglycerol and a free fatty acid by *Clupea harengus* L. larvae. J. Fish Biol. 67, 223–238. https://doi.org/10.1111/j.0022-1112.2005.00731.x.

Morais, S., Edvardsen, R.B., Tocher, D.R., Bell, J.G., 2012. Transcriptomic analyses of intestinal gene expression of juvenile Atlantic cod (*Gadus morhua*) fed diets with Camelina oil as replacement for fish oil. Comp. Biochem. Physiol. B Biochem. Mol. Biol. 161, 283–293. https://doi.org/10.1016/j.cbpb.2011.12.004.

Moroni, F., Naya-Català, F., Piazzon, M.C., Rimoldi, S., Calduch-Giner, J., Giardini, A., Martínez, I., Brambilla, F., Pérez-Sánchez, J., Terova, G., 2021. The effects of nisin-producing *Lactococcus lactis* strain used as probiotic on gilthead sea bream (*Sparus aurata*) growth, gut microbiota, and transcriptional response. Front. Mar. Sci. 8 https://doi.org/10.3389/fmars.2021.659519.

Morris, P.C., Gallimore, P., Handley, J., Hide, G., Haughton, P., Black, A., 2005. Full-fat soya for rainbow trout (*Oncorhynchus mykiss*) in freshwater: effects on performance, composition and flesh fatty acid profile in absence of hind-gut enteritis. Aquaculture 248, 147–161. https://doi.org/10.1016/j.aquaculture.2005.04.021.

Mourente, G., Dick, J.R., Bell, J.G., Tocher, D.R., 2005. Effect of partial substitution of dietary fish oil by vegetable oils on desaturation and β-oxidation of [1-^{14}C]18:3n-3 (LNA) and [1-^{14}C]20:5n-3 (EPA) in hepatocytes and enterocytes of European sea bass (*Dicentrarchus labrax* L.). Aquaculture 248, 173–186. https://doi.org/10.1016/j.aquaculture.2005.04.023.

Moutinho, S., Pedrosa, R., Magalhães, R., Oliva-Teles, A., Parisi, G., Peres, H., 2021. Black soldier fly (*Hermetia illucens*) pre-pupae larvae meal in diets for European seabass (*Dicentrarchus labrax*) juveniles: effects on liver oxidative status and fillet quality traits during shelf-life. Aquaculture 533, 736080. https://doi.org/10.1016/j.aquaculture.2020.736080.

Nogales-Mérida, S., Gobbi, P., Józefiak, D., Mazurkiewicz, J., Dudek, K., Rawski, M., Kierończyk, B., Józefiak, A., 2019. Insect meals in fish nutrition. Rev. Aquac. 11, 1080–1103. https://doi.org/10.1111/raq.12281.

Oxley, A., Jutfelt, F., Sundell, K., Olsen, R.E., 2007. Sn-2-monoacylglycerol, not glycerol, is preferentially utilised for triacylglycerol and phosphatidylcholine biosynthesis in Atlantic salmon (*Salmo salar* L.) intestine. Comp. Biochem. Physiol. B Biochem. Mol. Biol. 146, 115–123. https://doi.org/10.1016/j.cbpb.2006.09.007.

Priest, A.V., Koirala, R., Sivasankar, S., 2019. Single-molecule studies of classical and desmosomal cadherin adhesion. Curr. Opin. Biomed. Eng. 12, 43–50. https://doi.org/10.1016/j.cobme.2019.08.006.

Qian, B., Xue, L., Huang, H., 2016. Liver transcriptome analysis of the large yellow croaker (*Larimichthys crocea*) during fasting by using RNA-seq. PLoS ONE 11. https://doi.org/10.1371/journal.pone.0150240.

R Core Team, 2021. R: A Language and Environment for Statistical Computing. R Foundation for Statistical Computing, Vienna.

Rasmussen, R.S., 2001. Quality of farmed salmonids with emphasis on proximate composition, yield and sensory characteristics. Aquac. Res. 32, 767–786. https://doi.org/10.1046/j.1365-2109.2001.00617.x.

Reynolds, E.S., 1963. The use of lead citrate at high pH as an electron-opaque stain in electron microscopy. J. Cell Biol. 17 (1), 208–212. https://doi.org/10.1083/jcb.17.1.208.

Sitjà-Bobadilla, A., Alvarez-Pellitero, P., 1993. Pathologic effects of *Sphaerospora dicentrarchi* Sitjà-Bobadilla and Alvarez-Pellitero, 1992 and *S. Testicularis* Sitjà-Bobadilla and Alvarez-Pellitero, 1990 (Myxosporea: Bivalvulida) parasitic in the Mediterranean Sea bass *Dicentrarchus labrax* L. (Teleostei: Serranidae) and the cell-mediated immune reaction: a light and electron microscopy study. Parasitol. Res. 79, 119–129. https://doi.org/10.1007/BF00932257.

Soliman, N.F., Yacout, D.M.M., Hassaan, M.A., 2017. Responsible fishmeal consumption and alternatives in the face of climate changes. Int. J. Mar. Sci. https://doi.org/10.5376/ijms.2017.07.0015.

Soneson, C., Love, M.I., Robinson, M.D., 2016. Differential analyses for RNA-seq: transcript-level estimates improve gene-level inferences. F1000 Res. 4, 1–19. https://doi.org/10.12688/F1000RESEARCH.7563.2.

Sprague, M., Dick, J.R., Tocher, D.R., 2016. Impact of sustainable feeds on omega-3 long-chain fatty acid levels in farmed Atlantic salmon, 2006-2015. Sci. Rep. 6, 1–9. https://doi.org/10.1038/srep21892.

Stone, D.A.J., Oliveira, A.C.M., Ross, C.F., Plante, S., Smiley, S., Bechtel, P., Hardy, R.W., 2011. The effects of phase-feeding rainbow trout (*Oncorhynchus mykiss*) with canola oil and Alaskan Pollock fish oil on fillet fatty acid composition and sensory attributes. Aquac. Nutr. 17 https://doi.org/10.1111/j.1365-2095.2010.00792.x.

Tacchi, L., Secombes, C.J., Bickerdike, R., Adler, M.A., Venegas, C., Takle, H., Martin, S. A.M., 2012. Transcriptomic and physiological responses to fishmeal substitution with plant proteins in formulated feed in farmed Atlantic salmon (*Salmo salar*). BMC Genomics 13, 363. https://doi.org/10.1186/1471-2164-13-363.

Tibaldi, E., Hakim, Y., Uni, Z., Tulli, F., de Francesco, M., Luzzana, U., Harpaz, S., 2006. Effects of the partial substitution of dietary fish meal by differently processed soybean meals on growth performance, nutrient digestibility and activity of intestinal brush border enzymes in the European sea bass (*Dicentrarchus labrax*). Aquaculture 261, 182–193. https://doi.org/10.1016/j.aquaculture.2006.06.026.

Tocher, D.R., 2003. Metabolism and functions of lipids and fatty acids in teleost fish. Rev. Fish. Sci. 11, 107–184. https://doi.org/10.1080/713610925.

Tocher, D.R., 2015. Omega-3 long-chain polyunsaturated fatty acids and aquaculture in perspective. Aquaculture 449, 94–107. https://doi.org/10.1016/j.aquaculture.2015.01.010.

Torrecillas, S., Mompel, D., Caballero, M.J., Montero, D., Merrifield, D., Rodiles, A., Robaina, L., Zamorano, M.J., Karalazos, V., Kaushik, S., Izquierdo, M., Torrecillas, S., Mompel, D., Caballero, M.J., Montero, D., Merrifield, D., Rodiles, A., Robaina, L., Zamorano, M.J., Karalazos, V., Kaushik, S., Izquierdo, M., 2017. Effect of fishmeal and fish oil replacement by vegetable meals and oils on gut health of European sea bass (*Dicentrarchus labrax*). Aquaculture 468, 386–398. https://doi.org/10.1016/j.aquaculture.2016.11.005.

Torrecillas, S., Rimoldi, S., Montero, D., Serradell, A., Acosta, F., Fontanillas, R., Allal, F., Haffray, P., Bajek, A., Terova, G., 2023. Genotype x nutrition interactions in European sea bass (*Dicentrarchus labrax*): effects on gut health and intestinal microbiota. Aquaculture 574. https://doi.org/10.1016/j.aquaculture.2023.739639.

Torstensen, B.E., Nanton, D.A., Olsvik, P.A., Sundvold, H., Stubhaug, I., 2009. Gene expression of fatty acid-binding proteins, fatty acid transport proteins (cd36 and FATP) and β-oxidation-related genes in Atlantic salmon (*Salmo salar* L.) fed fish oil or vegetable oil. Aquac. Nutr. 15 (4), 440–451. https://doi.org/10.1111/j.1365-2095.2008.00609.x.

Tran, G., Heuzé, V., Makkar, H.P.S., 2015. Insects in fish diets. Anim. Front. 5, 37–44. https://doi.org/10.2527/af.2015-0018.

Turchini, G.M., Torstensen, B.E., Ng, W.K., 2009. Fish oil replacement in finfish nutrition. Rev. Aquac. 1, 10–57. https://doi.org/10.1111/j.1753-5131.2008.01001.x.

Turchini, G.M., Trushenski, J.T., Glencross, B.D., 2019. Thoughts for the future of aquaculture nutrition: realigning perspectives to reflect contemporary issues related to judicious use of marine resources in aquafeeds. N. Am. J. Aquac. 81, 13–39. https://doi.org/10.1002/naaq.10067.

UniProt Consortium, 2015. UniProt: a hub for protein information. Nucleic Acids Res. 43, D204–D212. https://doi.org/10.1093/nar/gku989.

UniProt Consortium, 2017. UniProt: the universal protein knowledgebase. Nucleic Acids Res. 45 (D1), D158–D169. https://doi.org/10.1093/nar/gkw1099.

Vandeputte, M., Gagnaire, P.A., Allal, F., 2019. The European sea bass: a key marine fish model in the wild and in aquaculture. Anim. Genet. 50, 195–206. https://doi.org/10.1111/age.12779.

Vogel, C., Marcotte, E.M., 2012. Insights into the regulation of protein abundance from proteomic and transcriptomic analyses. Nat. Rev. Genet. 13 (4), 227–232. https://doi.org/10.1038/nrg3185.

Wang, G., Bonkovsky, H.L., de Lemos, A., Burczynski, F.J., 2015. Recent insights into the biological functions of liver fatty acid binding protein 1. J. Lipid Res. 56 (12), 2238–2247. https://doi.org/10.1194/jlr.R056705.

Wang, A.R., Ran, C., Ringø, E., Zhou, Z.G., 2018. Progress in fish gastrointestinal microbiota research. Rev. Aquac. 10, 626–640. https://doi.org/10.1111/raq.12191.

Watanabe, T., 1982. Lipid nutrition in fish. Comp. Biochem. Physiol. B: Comp. Biochem. 73, 3–15. https://doi.org/10.1016/0305-0491(82)90196-1.

WHO, 2003. Joint WHO/FAO Expert Consultation. Diet, Nutrition and the Prevention of Chronic Diseases, WHO Technical Report Series 916 Geneva, Switzerland, p. 149.

Xu, H., Zhang, Y., Wang, C., Wei, Y., Zheng, K., Liang, M., 2017. Cloning and characterization of fatty acid-binding proteins (*fabps*) from Japanese seabass (*Lateolabrax japonicus*) liver, and their gene expressions in response to dietary arachidonic acid (ARA). Comp. Biochem. Physiol. B Biochem. Mol. Biol. 204, 27–34. https://doi.org/10.1016/j.cbpb.2016.11.006.

Yang, Y., Lundqvist, A., 2020. Immunomodulatory effects of IL-2 and IL-15; implications for cancer immunotherapy. Cancers 12 (12). https://doi.org/10.3390/cancers12123586.

Ye, W., Zheng, Y., Sun, Y., Li, Q., Zhu, H., Xu, G., 2023. Transcriptome analysis of the response of four immune related organs of tilapia (*Oreochromis niloticus*) to the addition of resveratrol in feed. Fish Shellfish Immunol. 133, 108510 https://doi.org/10.1016/J.FSI.2022.108510.

Zarantoniello, M., Randazzo, B., Gioacchini, G., Truzzi, C., Giorgini, E., Riolo, P., Gioia, G., Bertolucci, C., Osimani, A., Cardinaletti, G., Lucon-Xiccato, T., Milanović, V., Annibaldi, A., Tulli, F., Notarstefano, V., Ruschioni, S., Clementi, F., Olivotto, I., 2020. Zebrafish (*Danio rerio*) physiological and behavioural responses to insect-based diets: a multidisciplinary approach. Sci. Rep. 10 https://doi.org/10.1038/s41598-020-67740-w.

Zarantoniello, M., Oliveira, A.A.D., Sahin, T., Freddi, L., Torregiani, M., 2023. Enhancing rearing of European seabass (*Dicentrarchus labrax*) in aquaponic systems: investigating the effects of enriched black soldier fly (*Hermetia illucens*) prepupae meal on fish welfare and quality traits. Animals 13, 1921. https://doi.org/10.3390/ani13121921.

Zhao, L., Luo, J., Liu, Q., Du, J., Yang, H., Li, B., Zhou, Y., Yang, S., 2020. Different diets can affect the digestion and immunity of common carp (*Cyprinus carpio*) according to enzyme activity assay and transcriptome sequencing. Aquaculture 523, 735176. https://doi.org/10.1016/j.aquaculture.2020.735176.